



31 **Abstract:**

32 Nitrous acid (HONO) is an important precursor of OH radicals which affects not only the sinks
33 of primary air pollutants but also the formation of secondary air pollutants, whereas its source
34 closure in the atmosphere is still controversial due to a lack of experiment validation. In this
35 study, the HONO budget in Beijing has been analyzed and validated through the coronavirus
36 disease (COVID-19) lockdown event, which resulted in the largest changes in air pollutant
37 emissions in the history of modern atmospheric chemistry. A home-made Water-based Long-
38 Path Absorption Photometer (LOPAP) along with other instruments were used to measure the
39 HONO and related pollutants from January 1, 2020 to March 6, 2020, which covered the
40 Chinese New Year (CNY) and the COVID-19 lockdown. The average concentration of HONO
41 decreased from 0.97 ± 0.74 ppb before CNY to 0.53 ± 0.44 ppb during the COVID-19
42 lockdown, accompanied by a sharp drop of NO_x and the greatest drop of NO (around 87%).
43 HONO budget analysis suggests that vehicle emissions were the most important source of
44 HONO during the nighttime (53%) before CNY, well supported by the decline of their
45 contribution to HONO during the COVID-19 lockdown. We found that the heterogeneous
46 conversion of NO_2 on ground surfaces was an important nighttime source of HONO (31%),
47 while that on aerosol surfaces was a minor source (2%). Nitrate photolysis became the most
48 important daytime source during the COVID-19 lockdown compared with that before CNY,
49 resulting from the combined effect of the increase in nitrate and the decrease in NO. Our results
50 indicate that reducing vehicle emissions should be an effective measure for alleviating HONO
51 in Beijing.



52 **1. Introduction**

53 As the most vital oxidant in the troposphere, OH radicals not only govern the sink of most trace
54 compounds but also affect the production of secondary pollutants by initiating photochemical
55 reactions in the atmosphere. Nitrous acid (HONO) is an important primary precursor of OH
56 radicals (Kulmala and Petäjä, 2011; Zhang et al., 2023c). Photolysis of HONO can contribute
57 60% (Tan et al., 2018) and sometimes even 92% (Xue et al., 2020) to OH production in the
58 morning. Therefore, HONO can indirectly promote the formation of both secondary aerosols
59 (Zhang et al., 2019b) and ozone (Zhang et al., 2022a). In addition, HONO can react with
60 histamine to form carcinogens, such as nitrosamines, after entering the human body (Farren et
61 al., 2015). Thus, understanding the sources of HONO in the atmosphere has been a hot topic
62 for several decades, but it is still far from closed (Jiang et al., 2022).

63 Intensive studies have been carried out on HONO measurements and source analysis (Liu
64 et al., 2020c; Liu et al., 2020d; Zheng et al., 2020; Zhang et al., 2020; Xue et al., 2020; Zhang
65 et al., 2019a; Liu et al., 2019b). The concentrations of HONO in the atmosphere range from a
66 few ppt in remote areas (Spataro et al., 2016) to several ppb, even several tens ppb in heavily
67 polluted areas (Liu et al., 2019b; Liu et al., 2020c; Liu et al., 2020d; Zheng et al., 2020). The
68 sources of atmospheric HONO consist of direct emissions and secondary formation in the
69 atmosphere. Direct emissions include vehicles, soils, indoor air, livestock farming, and biomass
70 burning, while secondary formation includes gas-phase reaction between NO and OH radicals,
71 photolysis of particulate nitrate, and the heterogeneous reaction of NO₂ on ground and
72 particulate matter surfaces, including the photochemical heterogeneous reaction of NO₂.

73 Soil emissions, which depend on soil types, microorganisms, water content, temperature,



74 and pH (Kulmala and Petäjä, 2011; Weber et al., 2015; Kim and Or, 2019), are important
75 sources of HONO. They account for up to 80% of HONO sources, especially during
76 fertilization in agricultural areas (Liu et al., 2019c). Biomass burning, which often occurs in
77 the harvesting seasons of wheat/corn in summer and autumn (Zhang et al., 2019b; Sun et al.,
78 2017; Sun et al., 2018), even contributes 17% to HONO sources (Nie et al., 2015). Vehicle
79 emissions are considered an important source of HONO in traffic-intensive areas (Kramer et
80 al., 2020; Li et al., 2021) ranging from 8% to 80% of HONO sources (Fu et al., 2019; Xu et al.,
81 2015). This source is more important at nighttime compared with daytime (Zhang et al., 2016;
82 Fu et al., 2019; Liu et al., 2020d). Recently, indoor emissions have also been proposed as a
83 potential HONO source (Xue, 2022), which is related to the ventilation from high HONO
84 concentrations in indoor air to low HONO concentrations in outdoor air (Zhang et al., 2019b).
85 For example, the concentrations of HONO in urban areas increased by 0.6-0.8 ppb at night
86 after this source was accounted for in WRF-Chem model simulations (Zhang et al., 2019a).
87 Livestock farming is a previously overlooked source of HONO, especially in agricultural areas.
88 This emission can account for 39-45% of HONO production in rural areas (Zhang et al., 2023a).
89 Gas phase reaction between NO and OH, photolysis of nitrate particles, and light-enhanced
90 conversion of NO₂ are the main sources of daytime HONO (Liu et al., 2019c; Liu et al., 2020d;
91 Zhang et al., 2022b). The heterogeneous reaction of NO₂ on various surfaces is widely regarded
92 as an important source of HONO (Han et al., 2016; Liu et al., 2020b). Its contribution to
93 atmospheric HONO varied from 50% to 81% in different studies (Zheng et al., 2020; Liu et al.,
94 2019b; Fu et al., 2019).

95 Although intensive studies have been performed on HONO sources, the contributions of



96 different sources are still controversial (Zhou et al., 2011; Liu et al., 2014; Wu et al., 2019;
97 Kramer et al., 2020; Meng et al., 2020). For example, some studies reported that the
98 heterogenous reaction of NO₂ on ground surfaces was a main source of HONO, accounting for
99 ~42% of the observed HONO in Hong Kong and the Pearl River Delta (Xu et al., 2015; Zhang
100 et al., 2020). Vertical gradient measurements of HONO also showed that ground surfaces were
101 the main reaction surfaces (Pusede et al., 2015). However, some other studies suggested that
102 aerosol surfaces instead of ground surfaces were the main medium for NO₂ heterogeneous
103 production of HONO during the day in polluted areas in Beijing and Shanghai (Liu et al., 2014;
104 Cui et al., 2018; Meng et al., 2020). In particular, the heterogenous conversion of NO₂ to
105 HONO on aerosol surfaces was important under heavily polluted conditions (Meng et al., 2020;
106 Zhang et al., 2020). In contrast, some studies found that heterogeneous reaction was
107 unimportant compared to direct emissions (Tong et al., 2016; Hao et al., 2019; Zhang et al.,
108 2019b), accounting for only 5% to 8% of HONO sources (Kramer et al., 2020). For instance,
109 vehicle emissions can contribute around 40%-50% to Beijing's nighttime HONO sources
110 (Meng et al., 2020; Liu et al., 2020d). However, several studies found it to be an unimportant
111 HONO source, with a contribution ranging from 8% to 16% (Fu et al., 2019; Zheng et al., 2020;
112 Hao et al., 2019). It should be noted that the contribution of NO₂ heterogeneous reaction to
113 HONO greatly depends on the choice of NO₂ uptake coefficient (γ_{NO_2}), which varies from 10⁻
114 ⁸ to 10⁻⁴ in different studies (Meng et al., 2020; Liu et al., 2020b; Ge et al., 2019; Liu et al.,
115 2015; Liu et al., 2020d). Vehicle emissions also have similar characteristics because the HONO
116 emission rate strongly depends on the emission factor, i.e. the ratio of HONO/NO_x (Kramer et
117 al., 2020; R. Kurtenbach et al., 2001; Zhang et al., 2019c), which ranges from 0.03% to 2.1%



118 (Liao et al., 2021). For other HONO sources, the relative importance is affected by many
119 parameters, such as reaction kinetics for photolysis of nitrate, OH concentrations for
120 homogeneous reaction between NO and OH, emission fluxes for soil emissions, and so on.
121 Thus, the HONO budget still has a large uncertainty. In particular, it is an open question of how
122 to prove the importance of a specific reaction pathway or a source of atmospheric HONO.

123 Special events taking place on large spatial scales provide us with an alternative
124 opportunity to disclose the mysteries of the HONO budget because of obvious and potentially
125 large changes in some of the HONO sources. During the Spring Festival in 2020, the lockdown
126 measures during the new coronavirus disease -19 (COVID-19) pandemic led to a significant
127 reduction in primary emissions from traffic and industries. The magnitude and speed of changes
128 in air pollutant emissions have been considered the largest changes in the history of modern
129 atmospheric chemistry (Kroll et al., 2020). We conducted continuous field observations of
130 HONO and other air pollutants from January 1, 2020, to March 6, 2020, in downtown Beijing,
131 aimed at understanding the changes in HONO concentrations and sources during the lockdown
132 period compared to that before.

133 **2. Experimental section**

134 **2.1 Field measurements.**

135 Observations were carried out at the Aerosol and Haze Laboratory, Beijing University of
136 Chemical Technology (AHL/BUCT), which has been described in our previous work (Liu et
137 al., 2020d). Briefly, it is located on the west campus of BUCT, around 550 m from the west
138 third-ring road of Beijing, which is a typical urban observation site. The station is on the rooftop
139 of a 5-story building (about 18 m from the ground). HONO was measured with a homemade



140 Water-based Long-Path Absorption Photometer (LOPAP, Institute of Chemistry, Chinese
141 Academy of Sciences), which has been deployed in field observation studies (Tong et al., 2016;
142 Chen et al., 2020) and has been proven to be a stable and credible instrument for HONO
143 measurements (Crilley et al., 2019). The principle of this instrument is similar to that of a
144 commercial LOPAP (QUMA). Briefly, gas-phase HONO absorbed by deionized water (≥ 18.2
145 $M\Omega$) in a stripping coil reacts with N-(1-naphthyl) ethylenediamine-dihydrochloric acid (0.077
146 mmol L^{-1}) in an acidic solution (2 mmol L^{-1} sulfanilamide in 0.12 mol L^{-1} HCl) to form an azo
147 dye, which is measured at 550 nm with a spectrometer equipped with a LWCC (Liquid
148 Waveguide Capillary Cell, LWCC-3250, WPI, USA). The sampling rate was 1 L min^{-1}
149 controlled by a flow meter and a diaphragm pump. The flow rate of absorption liquid was 0.5
150 ml min^{-1} controlled by a peristaltic pump. The limit of detection of the LOPAP was 0.01 ppb
151 for a sampling duration of 60 s . The instrument was calibrated with nitrite standard solution
152 before and after each measurement about every three weeks and calibrated by zero air every
153 24 hours to check zero drift. An overestimation of HONO concentration (6.7%), calibrated in
154 control experiments with 100 ppb of NO_2 at $50\% \text{ RH}$ due to the interference of NO_2 in the
155 sampling inlet (about 30 cm of Teflon tube), was accounted for when we calculating the HONO
156 concentrations in this work.

157 A set of commercial analyzers for NO_x , SO_2 , CO , and O_3 (Thermo Scientific 42i, 43i, 48i,
158 49i) were also available. $\text{PM}_{2.5}$ was measured using a Tapered Element Oscillating
159 Microbalance (TEOM, Thermo Fisher Scientific, 1405). The chemical composition of non-
160 refractory $\text{PM}_{2.5}$ (NR- $\text{PM}_{2.5}$) was measured using a Time-of-flight Aerosol Chemical
161 Speciation Monitor (ToF-ACSM, Aerodyne). Meteorological parameters including



162 temperature, RH, pressure, wind speed and direction, and ultraviolet radiation (A and B) were
163 measured using a weather station (AWS 310 at AHL/BUCT station, Vaisala). The planetary
164 boundary layer (PBL) height and visibility were measured using a ceilometer (CL51, Vaisala)
165 and a visibility sensor (PWD22, Vaisala), respectively. The photolysis rate (J_{NO_2}) was measured
166 via a continuous measurement of the actinic flux in the wavelength range of 285-375 nm using
167 a J_{NO_2} filter-radiometer (2-pi- J_{NO_2} radiometer, Metcon). All instruments used in the
168 measurement as well as their detection limits are shown in Table S1.

169 **2.2 HONO budget calculation.**

170 Potential sources of HONO include direct emissions (vehicle emissions, soil emissions, indoor
171 emissions, biomass combustion), the gas-phase reaction between NO and OH radicals, the
172 photolysis of nitrate in particulate matter, and the heterogeneous reaction of NO_2 on the ground
173 and particulate matter surfaces. The sources including vehicle emissions ($E_{vehicle}$), soil
174 emissions (E_{soil}), the reaction of NO and OH (P_{NO-OH}), the photolysis of particulate nitrate
175 ($P_{nitrate}$), and the heterogeneous reaction of NO_2 ($P_{aerosol}$ and P_{ground}) have been accounted
176 for. At present, there are relatively few studies on indoor emissions. Biomass combustion is an
177 unimportant HONO source in downtown Beijing in winter according to a previous study
178 (Zhang et al., 2019b). Thus, these two sources are not accounted for in this work. The major
179 sinks of HONO, including dry deposition ($L_{deposition}$), the homogeneous reaction with OH
180 radicals ($L_{HONO-OH}$), photolysis ($L_{photolysis}$), and vertical and horizontal transport (T_{trans}),
181 are considered.

182 The calculation method and details in parameterization are shown in Table 1. Briefly, the
183 budget and estimated concentration of HONO can be calculated according to the following



184 equations,

$$185 \quad \frac{dC_{HONO}}{dt} = E_{soil} + E_{vehicle} + P_{NO-OH} + P_{nitrate} + P_{aerosol} + P_{ground} -$$

$$186 \quad L_{photolysis} - L_{HONO-OH} - L_{deposition} - T_{trans} \quad (1)$$

$$187 \quad HONO_{est,t_2} = HONO_{obs,t_1} + Sources_{t_2} - Sinks_{t_2} \quad (2)$$

188 where $\frac{dC_{HONO}}{dt}$ is the change rate of HONO mixing ratios (ppb h⁻¹), $HONO_{est,t_2}$ is the
 189 estimated concentration of HONO at time t_2 , while $HONO_{obs,t_1}$ is the observed concentration
 190 of HONO at time t_1 . The input parameters for the parameterization scheme are detailed in Table
 191 S2 (M0).

192 The emission rate (E_{HONO} , ppb h⁻¹) of soil and vehicle were calculated based on the
 193 emission flux (F_{HONO} , g m⁻² s⁻¹), the PBL height (H , m), and the conversion factor (α). For
 194 vehicle emissions, according to our previous research at the same site, the emission factor (EF,
 195 HONO/NO_x) was selected as 1.09% (Liu et al., 2020d), which is comparable to the actual
 196 values in Hong Kong ($1.2 \pm 0.4\%$ and $1.24 \pm 0.35\%$) (Liang et al., 2017; Xu et al., 2015),
 197 Guangzhou (1.0%) (Li et al., 2012), Beijing (1.3% and 1.41%) (Zhang et al., 2019c; Meng et
 198 al., 2020), and other places. For secondary formation, the calculation of the production rate
 199 (P_{HONO} , ppb h⁻¹) is shown in Table 1, in which k_1 is the rate constant of the quasi-first order
 200 reaction (s⁻¹), $C_{precursor}$ is the concentration of the precursor (ppb). For the heterogeneous
 201 reaction of NO₂, we calculated the conversion rate in the light of Eqs. (3)-(5):

$$202 \quad k_{het}^0 = \frac{C_{HONO,corr,t_2} - C_{HONO,corr,t_1}}{C_{NO_2} \times (t_2 - t_1)} \quad (3)$$

$$203 \quad k_{het}^{CO} = \frac{2 \times \left[\frac{C_{HONO,corr,t_2} \times \overline{C_{CO}}}{C_{CO,t_2}} - \frac{C_{HONO,corr,t_1} \times \overline{C_{CO}}}{C_{CO,t_1}} \right]}{(t_2 - t_1) \times \left[\frac{C_{NO_2,t_2}}{C_{CO,t_2}} + \frac{C_{NO_2,t_1}}{C_{CO,t_1}} \right] \times \overline{C_{CO}}}$$



204
$$= \frac{2 \times \left[\frac{C_{HONO,corr,t_2}}{C_{CO,t_2}} - \frac{C_{HONO,corr,t_1}}{C_{CO,t_1}} \right]}{(t_2 - t_1) \times \left[\frac{C_{NO_2,t_2}}{C_{CO,t_2}} + \frac{C_{NO_2,t_1}}{C_{CO,t_1}} \right]} \quad (4)$$

205
$$k_{het} = \frac{1}{2} \times (k_{het}^0 + k_{het}^{CO}) \quad (5)$$

206 where k_{het} is the quasi-first-order rate constant of the transformation to HONO (s^{-1}), k_{het}^0
 207 and k_{het}^{CO} are the reaction rate constants after uncalibrated and CO calibrated, respectively
 208 (Zhang et al., 2020). $\overline{C_{NO_2}}$ and $\overline{C_{CO}}$ are the mean concentration of NO_2 and CO from t_1 to t_2 .
 209 $C_{CO,t}$ and $C_{NO_2,t}$ are mixing ratios of CO and NO_2 , respectively, at the measuring time t .
 210 $C_{HONO,corr,t}$ (ppb) is the HONO concentration corrected after subtracting the primary
 211 emissions (including vehicle and soil emissions, and the HONO produced by the homogeneous
 212 reaction of NO and OH and the photolysis of nitrate) at the measuring time t according to Eq.
 213 (6):

214
$$C_{HONO,corr,t} = C_{HONO,t} - E_{soil,t} - E_{vehicle,t} - P_{NO-OH,t} - P_{nitrate,t} \quad (6)$$

215 it is worth noting that the $C_{HONO,corr}$ only accounted for vehicle exhausts in previous HONO
 216 budget studies. This may overestimate the contribution of heterogeneous reactions to HONO
 217 sources because other emission sources and homogeneous reactions should also contribute to
 218 HONO.

219 Meanwhile, when estimating the upper limit of the contribution of heterogeneous
 220 reactions, we take a small conversion factor (HONO/ NO_x) of 0.4% as the lower limit of vehicle
 221 emissions, in contrast to the normal value of 1.09% (Liu et al., 2020d). We normalize the
 222 EI_{NO_x} caused by the vehicle with the measured C_{NO_x} during the observations. This method
 223 has also been widely used in previous studies (Liu et al., 2019b; Li et al., 2018). In addition,
 224 soil emissions are calculated using the lower limit (Oswald et al., 2013). The mean value of



225 k_{het} during the BCNY (before the Chinese New Year) was 0.0051 h^{-1} , while it was 0.006 h^{-1}
226 in the COVID-19 lockdown, which are consistent with previous studies, such as Ji'nan (0.0068
227 h^{-1}) (Li et al., 2018) and Shanghai (0.007 h^{-1}) (Wang et al., 2013), while less than those in
228 Shijiazhuang (0.016 h^{-1}) (Liu et al., 2020c), Kathmandu (0.014 h^{-1}) (Yu et al., 2009), and
229 Guangzhou (0.016 h^{-1}) (Qin et al., 2009).



230

Table 1. Summary of parameters for HONO sources and sinks

HONO formation/loss pathways	Calculations	Parameters	Reference
Soil emissions → HONO		$F_{\text{HONO,soil}}$	1
Vehicle emissions → HONO	$E_{\text{HONO}} = \alpha \times F_{\text{HONO}}/H$	$F_{\text{HONO,vehicle}} = (EI_{\text{NO}_x,\text{vehicle}}/A) \times (\text{HONO}/\text{NO}_x)_{\text{vehicle}}$	2
NO + OH → HONO		$k_{\text{NO-OH}} = 7.2 \times 10^{-12} \text{ cm}^3 \text{ molecule}^{-1} \text{ s}^{-1}$	3
$\text{NO}_3^- \xrightarrow{h\nu} \text{HONO}$		$J_{\text{NO}_3^-} = 8.24 \times 10^{-5} / 3.59 \times 10^{-7} \times J_{\text{HNO}_3,\text{MCM}}$	
$\text{NO}_2 + \text{H}_2\text{O} \xrightarrow{\text{aerosol surface}} \text{HONO}$	$P_{\text{HONO}} = 3600 \times k \times c_{\text{precursor}}$	$k_{\text{het}} = (\gamma_{\text{NO}_2} \times A_s \times \omega / 4) \times Y_{\text{HONO}}$	4
$\text{NO}_2 + \text{H}_2\text{O} \xrightarrow{\text{ground surface}} \text{HONO}$		$k_{\text{het}} = (\gamma_{\text{NO}_2} \times \delta \times \omega / 4H) \times Y_{\text{HONO}}$	
$\text{HONO} \xrightarrow{h\nu} \text{NO} + \text{OH}$	$L_{\text{photolysis}} = 3600 \times J_{\text{HONO}} \times c_{\text{HONO}}$	$J_{\text{HONO,MCM}}$	
$\text{HONO} + \text{OH} \rightarrow \text{H}_2\text{O} + \text{NO}_2$	$L_{\text{HONO-OH}} = 3600 \times k_{\text{HONO-OH}} \times c_{\text{HONO}} \times c_{\text{OH}}$	$k_{\text{HONO-OH}} = 6 \times 10^{-12} \text{ cm}^3 \text{ molecule}^{-1} \text{ s}^{-1}$	5
HONO deposition	$L_{\text{deposition}} = (3600 \times V_d \times c_{\text{HONO}}) / H$	$V_d = 0.001 \text{ m s}^{-1}$	6
HONO transport (vertical and horizontal)	$T_{\text{trans}} = k_{\text{dilution}} \times (c_{\text{HONO}} - c_{\text{HONO,background}})$	$k_{\text{dilution}} = 0.23 \text{ h}^{-1}$	7

$F_{\text{HONO,soil}}$ (soil emission flux) was calculated by the temperature-dependent HONO emission flux on grasslands with a water content of 35% to 45%. A is the urban area of Beijing, $EI_{\text{NO}_x,\text{vehicle}}$ is the emission inventory of NO_x from vehicle (g s^{-1}). The calculation of the HONO emission flux, during BCNY, was based on the hourly NO_x emission inventory of Beijing vehicles ($F_{\text{HONO}} = F_{\text{NO}_x} \times (\text{HONO}/\text{NO}_x)_{\text{vehicle}}$), while during COVID-19, it was combined with the hourly average traffic index (www.nitrafficindex.com). The $(\text{HONO}/\text{NO}_x)_{\text{vehicle}}$ was selected as 1.09% (Liu et al., 2020d). The OH concentration was estimated using the same method as in the previous study (Liu et al., 2020c). The mean photolysis frequency of nitrate ($J_{\text{NO}_3^-}$) was normalized to the measured UV light intensity. A_s is the surface area concentration of the reaction surface ($\text{m}^2 \text{ m}^{-3}$); ω is the average molecular velocity (m s^{-1}); γ is the uptake coefficient of the precursor, was assumed to be 2×10^{-6} ; Y_{HONO} is the yield of HONO. δ is the surface roughness, in this study, we used 3.85 for our calculation (Liu et al., 2020d). c_{HONO} and $c_{\text{HONO,background}}$ is the HONO concentration at the observation site and background site, respectively.

1: (Oswald et al., 2013). 2: (Yang et al., 2019). 3: (Liu et al., 2020c). 4: (Liu et al., 2020d). 5: (Kanaya et al., 2007). 6: (Han et al., 2017b). 7: (Dillon et al., 2002).

231



232 We further derived the uptake coefficient of NO₂ (γ_{NO_2}) on both ground and particle
233 surfaces according to Eq. (7).

$$234 \quad k_{het} = \frac{\gamma_{NO_2} \times A_s \times \omega}{4} \times Y_{HONO} \quad (7)$$

235 The calculated γ_{NO_2} ranged from 1×10^{-6} to 3×10^{-6} . Therefore, we choose
236 2×10^{-6} to calculate the heterogeneous yield of NO₂, which is comparable with those derived
237 in urban environments like Ji'nan (1.4×10^{-6}) (Li et al., 2018) and the laboratory experiments
238 (10^{-7} to 10^{-6}) (Han et al., 2013; Stemmler, 2007; Han et al., 2017a) on different particles, but
239 lower than the uptake coefficient of 10^{-5} reported in other studies (Zhang et al., 2020; Ge et al.,
240 2019).

241 The OH concentration was calculated according to Eq. (8), which is based on the function
242 of the photolysis rates (J) of O₃ and NO₂, and the NO₂ mixing ratio (C_{NO_2}).

$$243 \quad C_{OH} = \frac{4.1 \times 10^9 \times (J_{NO_2})^{0.19} \times (J_{O_3})^{0.83} \times (140 C_{NO_2} + 1)}{0.41 C_{NO_2}^2 + 1.7 C_{NO_2} + 1} \quad (8)$$

244 Notably, this parameterization scheme was developed based on measurements at rural sites
245 (Ehhalt and Rohrer, 2000), where NO_x concentrations were lower than in urban environments.
246 Alicke et al. (Alicke, 2002) found that OH concentrations estimated with this scheme were in
247 good agreement with those calculated according to a pseudo-steady state method during the
248 pollution period in urban environments (such as Milan), although some uncertainty was
249 expected. In our previous study (Liu et al., 2020d), we also found that the estimated OH
250 concentrations using this method were comparable with those observed values in the North
251 China Plain (Tan et al., 2019). Thus, daytime OH concentrations estimated using this method
252 should be overall credible although the uncertainty is inevitable. The nocturnal OH
253 concentration in North China generally varied from 1.0×10^5 molecules cm⁻³ (Ma et al., 2019;



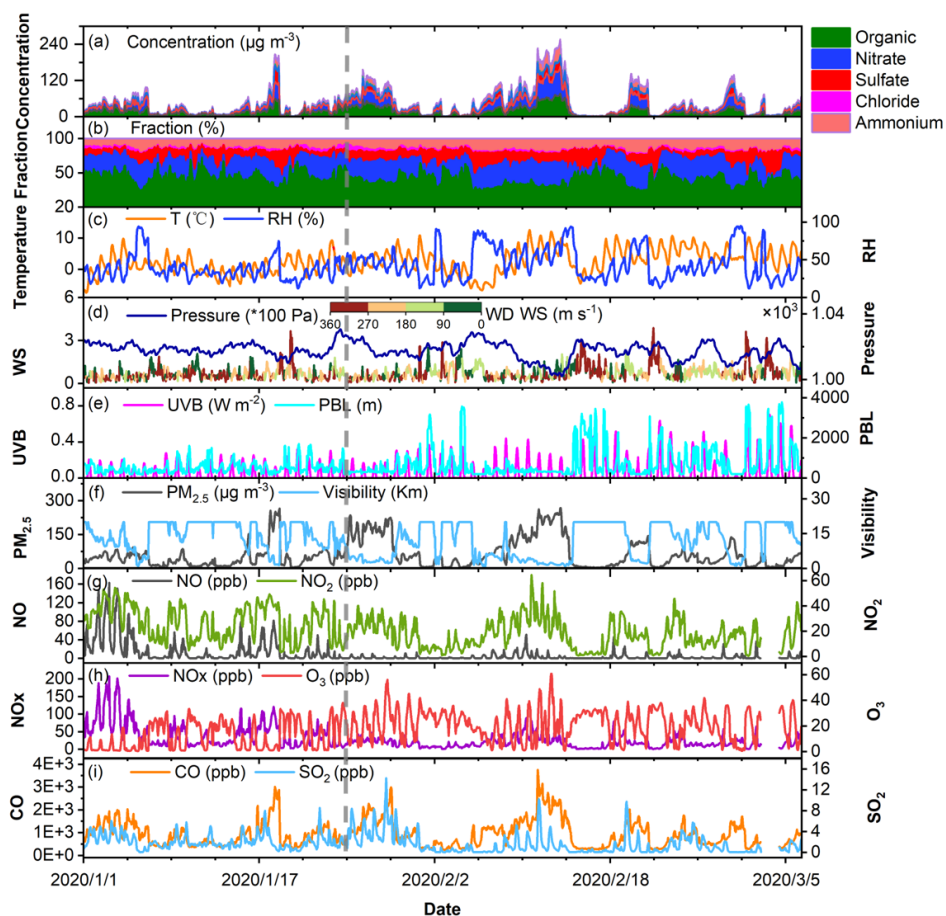
254 Tan et al., 2018) in winter to 5×10^5 molecules cm^{-3} in summer (Tan et al., 2017; Tan et al.,
255 2020). We further parameterized the nocturnal OH concentrations according to atmospheric
256 temperature to reflect the seasonal variations of OH concentration. Fig S1 summarizes the
257 observed OH concentrations in the North China Plain. The results estimated in this study are
258 slightly lower than those observed in Wangdu, but almost consistent with those in Beijing and
259 Huairou. In summary, we should be optimistic about the estimation of OH concentration. Then
260 a sensitivity analysis was performed to understand the influence of the uncertainty of OH
261 concentration on HONO sources as discussed in Section 3.3.

262 The loss rate of HONO, including dry deposition ($L_{deposition}$), homogeneous reaction
263 with OH radicals ($L_{HONO-OH}$), photolysis ($L_{photolysis}$), and vertical and horizontal transport
264 (T_{trans}), were calculated using the equations shown in Table 1. Where J_{HONO} is the photolysis
265 rate of HONO (s^{-1}), $k_{HONO-OH}$ is the second-order reaction rate constant between HONO and
266 OH, V_d is the dry deposition rate of HONO, and $K_{dilution}$ is the dilution rate (including both
267 vertical and horizontal transport). The details are described in our previous work (Liu et al.,
268 2020c; Liu et al., 2020d).

269 3. Results and discussion

270 3.1 Air quality during observations.

271 Figure 1 shows the time series of the concentration and relative proportion of non-refractory
272 components in $\text{PM}_{2.5}$, trace gases (SO_2 , O_3 , CO , NO , NO_2 , and NO_x), and meteorological
273 parameters (temperature, relative humidity (RH), and pressure). We divide the sampling period
274 into two sub-periods, i.e., P1 from January 1 to January 24 (BCNY, before the Chinese New
275 Year) and P2 from January 25 to March 6 (COVID-19 lockdown).



276

277 **Figure 1.** An overview of the measurement of the mass concentrations of the different
 278 components of non-refractory-PM_{2.5} (NR-PM_{2.5}), the mass fraction of the individual
 279 components, PM_{2.5}, and meteorological parameters, NO_x (NO, NO₂), O₃, CO and SO₂ in 1-hour
 280 average from 1 January to 6 March 2020. Meteorological parameters consist of visibility, PBL
 281 heights, UVB, wind speed, wind direction, Pressure, RH, and temperature. The observations
 282 are divided into two phases (P1:2020.01.01-2020.01.24 and P2:2020.01.25-2020.03.06).

283

284 It can be seen from Fig. 1 that during P1, there was only one heavy pollution incident



285 lasting one to two days, while there were two serious pollution events lasting more than two
286 days ($PM_{2.5} > 75 \mu g m^{-3}$) in the P2 stage. Table S3 summarizes the statistical results of the wind
287 speed, $PM_{2.5}$, RH, T, HONO, trace gases, and NR- $PM_{2.5}$ for the entire measurement period.
288 During P1, the concentration of $PM_{2.5}$ varied between 0.2-288 $\mu g m^{-3}$ and the mean
289 concentration was $47.2 \pm 44.5 \mu g m^{-3}$. In contrast, the $PM_{2.5}$ concentrations varied from 0.3 to
290 258 $\mu g m^{-3}$ with a mean value of $69.9 \pm 67.2 \mu g m^{-3}$ during P2. The concentrations of SO_2 were
291 in the range of 0.02-8.56 ppb with a mean value of 2.09 ± 1.35 ppb in P1, while it varied from
292 0.01 to 14.23 ppb with the mean concentration of 1.49 ± 1.99 ppb during P2, suggesting slightly
293 decreased contribution of coal combustion during P2 (Fig. 1i). This is similar to that reported
294 by Cui et al (Cui et al., 2020) and Shen et al (Shen et al., 2021). The mean concentrations of
295 NO_x decreased significantly ($P < 0.05$) from 45.35 ± 38.86 ppb in P1 to 19.44 ± 14.42 ppb in
296 P2, dropping by about 57%. This is close to the reduction amplitude (50%) reported by Wang
297 et al. (Wang et al., 2020a) but lower than that (76%) proposed by Lv et al (Lv et al., 2020). In
298 particular, the NO mean concentrations dropped from 18.42 ± 29.24 ppb (ranging from 0.03 to
299 163 ppb) in P1 to 2.4 ± 5.46 ppb (ranging from 0.01 to 51 ppb). The average hourly
300 concentration of NO_2 in the P1 phase was 26.9 ± 13.4 ppb, while it was 17.18 ± 11.3 ppb in P2.
301 The NO_2 concentration dropped by about 36% from P1 to P2, which is similar to the recently
302 reported findings (ranging from 36% to 53%) (Zhao et al., 2020; Wang et al., 2020b; Wang et
303 al., 2021). According to the emission inventory of NO_x , traffic and industry contributed 46.7 %
304 and 31.3% to NO_x emissions in Beijing, respectively (Zheng et al., 2014). This means the
305 decrease in NO_x concentration should be explained by both reductions in traffic and industrial
306 emissions (Lv et al., 2020; Wang et al., 2020a; Zhao et al., 2020). In particular, traffic emissions



307 during P2 should play an important role in local NO reduction. However, as the temperature
308 and ultraviolet light irradiation increased and the NO_x concentration decreased (Kroll et al.,
309 2020; Le et al., 2020), the average concentration of O₃ during P2 was 21.31 ± 11.73 ppb, which
310 was significantly higher than 12.16 ± 10.79 ppb during P1. This result is similar to the 71.4%
311 increase in O₃ in Shijiazhuang during the same period (Liu et al., 2020c). In addition, it can be
312 seen from Fig. 1 that the change trends of PM_{2.5} and CO are synchronized, which also means
313 that both primary emissions and secondary generation contribute to the accumulation of PM_{2.5}
314 concentration (Liu et al., 2020c).

315 All the major components of PM_{2.5}, including sulfate, nitrate, ammonium, chloride, and
316 organic aerosol, increased obviously in P2 compared to P1. Throughout the entire observation
317 period, organic matter and nitrate dominated the composition of PM_{2.5}. The proportion of
318 nitrate in inorganic salts increased to 31.2% in P2, up from 28.1% in P1. Although the sulfate
319 concentration increased, its proportion within inorganic salts slightly decreased on haze days,
320 going from 16.5% in P1 to 15.2% in P2. Thus, the ratio of NO₃⁻ to SO₄²⁻ during pollution events
321 increased significantly from 1.76 in P1 to 2.10 in P2. This is similar to previous findings
322 reported by Sun (Sun et al., 2020). These findings suggest that the decrease in anthropogenic
323 emissions during the P2 period resulted in a significant reduction in gas precursors (Table S3),
324 but it did not lead to a corresponding reduction in secondary aerosol species during periods of
325 pollution. This is supported by the increased potential secondary aerosol formation under
326 pollution conditions (Sun et al., 2020). For example, higher values of the SOR (sulfur oxidation
327 ratio, molar fraction of sulfate in total sulfur including sulfate and SO₂) and NOR (nitrogen
328 oxidation ratio, molar fraction of nitrate in total nitrogen, including nitrate and NO₂), i.e., 0.63



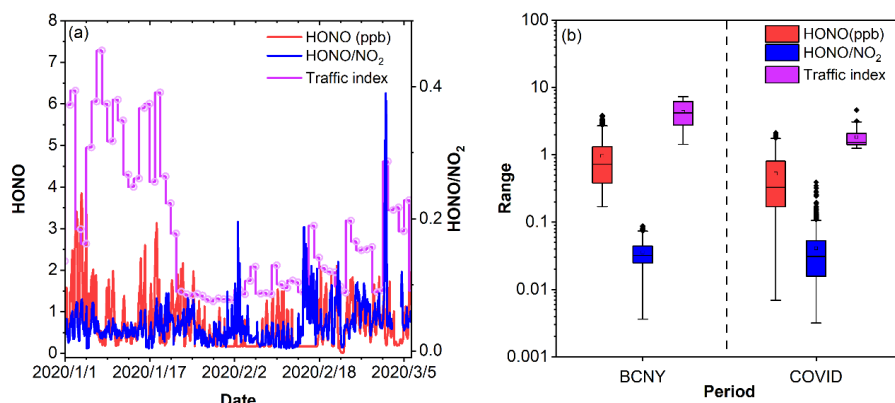
329 and 0.34, were observed in P2 than those (0.48 and 0.14) in P1. Under stagnant weather
330 conditions (wind speed $< 2 \text{ m s}^{-1}$), higher temperatures and RH as shown in Table S3 might
331 facilitate the conversion from precursors into particles (Liu et al., 2020d). The above results
332 indicate that the air pollution dominated by secondary formation is much more serious in P2,
333 which is supported by both the increased concentration and the greater number of pollution
334 days in P2 than in P1, even though primary emissions decreased obviously.

335 **3.2 Influence of Chinese New Year and the COVID-2019 epidemic event on HONO**
336 **concentration in Beijing.**

337 Figure 2 displays the time series of the HONO concentration, the HONO/NO₂ ratio, and the
338 traffic index (www.nitrafficindex.com). In Fig. 2b, there is a significant decrease in the traffic
339 index, indicating reduced traffic congestion during the COVID-19 lockdown (P2 period)
340 compared to the P1 period. The HONO/NO₂ ratio is frequently used to indicate the conversion
341 of NO₂ to HONO through heterogeneous reactions (Sun et al., 2013). A higher HONO/NO₂
342 indicates that the heterogeneous conversion process plays a more significant role in HONO
343 production. However, as depicted in Fig. 2b, both the traffic index and HONO exhibit a similar
344 decreasing trend, while the HONO/NO₂ ratio remains relatively stable. Notably, both the traffic
345 index and the NO concentration experienced a steep decline after January 24, coinciding with
346 a significant decrease in HONO concentration. Furthermore, as shown in Fig. S2, there is a
347 strong correlation between HONO and NO_x in both P1 and P2. However, HONO concentration
348 does not track PM_{2.5} concentration well. These results imply that HONO might be more
349 influenced by vehicle emissions than by heterogeneous reactions. This contrasts with prior
350 studies that heterogeneous reactions on aerosol surfaces are the primary source of HONO in



351 pollution events in Beijing (Liu et al., 2014; Cui et al., 2018; Meng et al., 2020).



352

353 **Figure 2.** (a) Times series of HONO, traffic index, and HONO/NO₂, (b) Box plots of HONO,
354 HONO/NO₂, and the traffic index in Beijing during different periods (BCNY=P1, LOCK=P2).

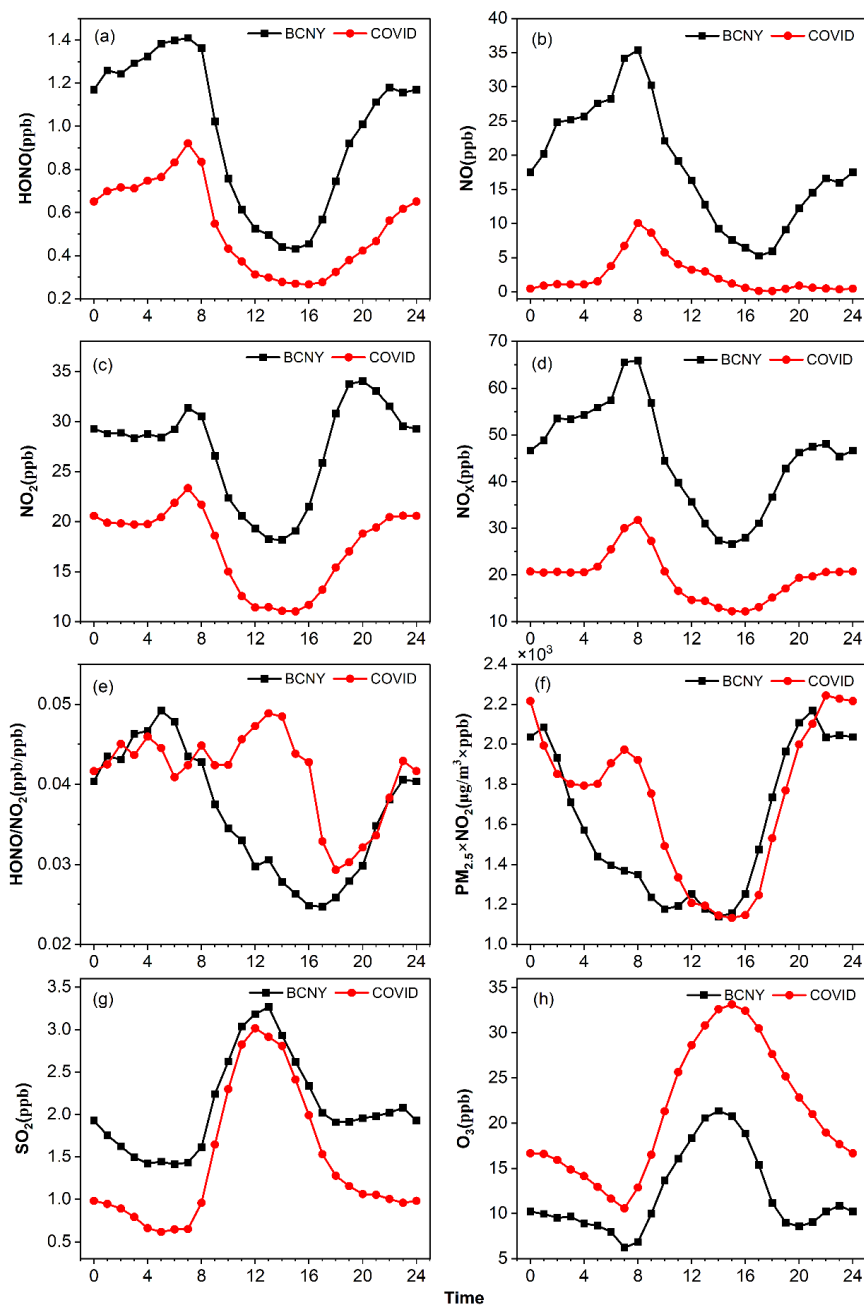
355

356 Table S4 summarizes the mean concentrations of HONO, NO₂, NO, and PM_{2.5} over the
357 two periods in this study as well as the data reported in previous studies. During P1, HONO
358 concentration ranged from 0.17 to 3.85 ppb, with a mean value of 0.97 ± 0.74 ppb. This
359 concentration is similar to previous observations, such as in Beijing, Xi'an, Jinan, Shanghai,
360 Hong Kong, and Rome, which all ranged from 0.95 to 1.15 ppb (Acker et al., 2006; Wang et
361 al., 2013; Xu et al., 2015; Huang et al., 2017; Liu et al., 2020d; Li et al., 2018). However, during
362 the COVID-19 lockdown, the HONO concentration decreased to 0.53 ± 0.44 ppb, representing
363 a drop of 45.3% compared with that in BCNY. This value is comparable to the concentrations
364 reported in the literature for clean days in December 2016 in Beijing (0.5 ± 0.2 ppb) and in the
365 winter of 2018 in Xiamen (0.52-0.61 ppb). At the same time, as discussed in the previous
366 section, the NO concentration decreased by nearly 87% from BCNY to COVID-19 lockdown,
367 and the NO₂ concentration dropped by about 36%. Consequently, we can conclude that the



368 concentrations of HONO, NO, and NO₂ were the most affected pollutants during the COVID-
369 19 lockdown period.

370 Figure 3 shows the diurnal curves of HONO, NO_x, NO, NO₂, HONO/NO₂, O₃, SO₂, and
371 PM_{2.5}×NO₂ during P1 (BCNY) and P2 (COVID-19 lockdown). The black and red lines
372 represent P1 and P2, respectively. HONO shows a similar trend in both periods. After sunset,
373 HONO began to accumulate due to the attenuation of solar radiation and the development of
374 the boundary layer, reaching maximum values of 1.41 ± 0.83 ppb and 0.92 ± 0.64 ppb around
375 7:00 during P1 and P2, respectively. Subsequently, due to the impact of the boundary layer and
376 rapid photolysis, the HONO concentration gradually decreased and remained at a low level
377 until sunset, with the corresponding minimum value of 0.43 ± 0.24 ppb and 0.27 ± 0.17 ppb at
378 about 15:00. Similar to HONO, the NO₂ concentration shows an upward trend during the
379 morning rush hour. Its peak appeared at 7:00 (BCNY: 31.4 ± 9.23 ppb; COVID-19 lockdown:
380 23.3 ± 10.74 ppb), and then dropped rapidly and remained at a low level due to photochemical
381 processes and the development of the boundary layer. The minimum concentration occurs
382 around 14:00 to 15:00 (BCNY: 18.17 ± 10.69 ppb; COVID-19 lockdown: 11.0 ± 7.64 ppb).
383 After sunset, NO₂ began to increase again. It is worth noting that during BCNY, both NO₂ and
384 NO exhibited a prominent evening peak, whereas there was no such evening peak during the
385 COVID-19 lockdown. Thus, NO_x and NO₂ had similar changing trends, i.e., the morning peak
386 observed in both periods with the highest mean values of 65.93 ± 50.37 ppb and 31.7 ± 21.47
387 ppb in BCNY and COVID-19 lockdown, respectively.



388

389 **Figure 3.** Diurnal variation of HONO, NO, NO₂, NO_x, HONO/NO₂, PM_{2.5}×NO₂, SO₂, O₃. The

390 black lines are the diurnal curves before CNY and the red ones are during the COVID-19



391 lockdown.

392

393 NO and HONO showed a similar trend in P1. They began to decline continuously after
394 sunrise and continued to rise after sunset. The peaks of NO were 35.40 ± 43.55 ppb and $10.0 \pm$
395 12.67 ppb in P1 and P2, respectively. It is worth noting that the upward trend of NO
396 concentration in the afternoon of the P2 stage was not obvious, as the absolute concentration
397 of NO was very low. O₃ and HONO showed opposite diurnal curves, with the maximum O₃
398 concentrations occurring in the afternoon, which were 21.35 ± 9.31 ppb and 33.14 ± 10.26 ppb
399 in P1 and P2, respectively. SO₂ and O₃ exhibited similar trends, with the maximum values in
400 P1 and P2 were 3.26 ± 2.19 ppb and 3.01 ± 3.06 ppb at 13:00, and their lowest values were
401 1.41 ± 0.68 ppb and 0.62 ± 0.82 ppb at 5:00 or 6:00.

402 Previous studies proposed that the heterogeneous reactions of NO₂ on the aerosol surface
403 play an important role in HONO production. Specifically, this pathway was considered the
404 major source of HONO on polluted days (Cui et al., 2018; Meng et al., 2020; Zhang et al.,
405 2020). PM_{2.5}×NO₂ can be used as an indicator for the heterogeneous reaction of NO₂ on the
406 surface of aerosols (Cui et al., 2018). It was found that the value of PM_{2.5}×NO₂ in P2 ($1697 \pm$
407 2142) was slightly higher than that in P1 (1583 ± 1967). In the early morning, the product of
408 PM_{2.5} and NO₂ in the P2 stage was even higher than that in the P1 stage. On the other hand, the
409 ratio of HONO/NO₂ is usually used to evaluate the formation of HONO during the conversion
410 of NO₂. As shown in Fig. 3, in the P1 stage, the HONO/NO₂ ratio shows a similar daily trend
411 to HONO, which began to rise after sunset and reached a peak at night and then decreased in
412 the early morning due to the increase of NO₂ concentrations and the photolysis of HONO. In



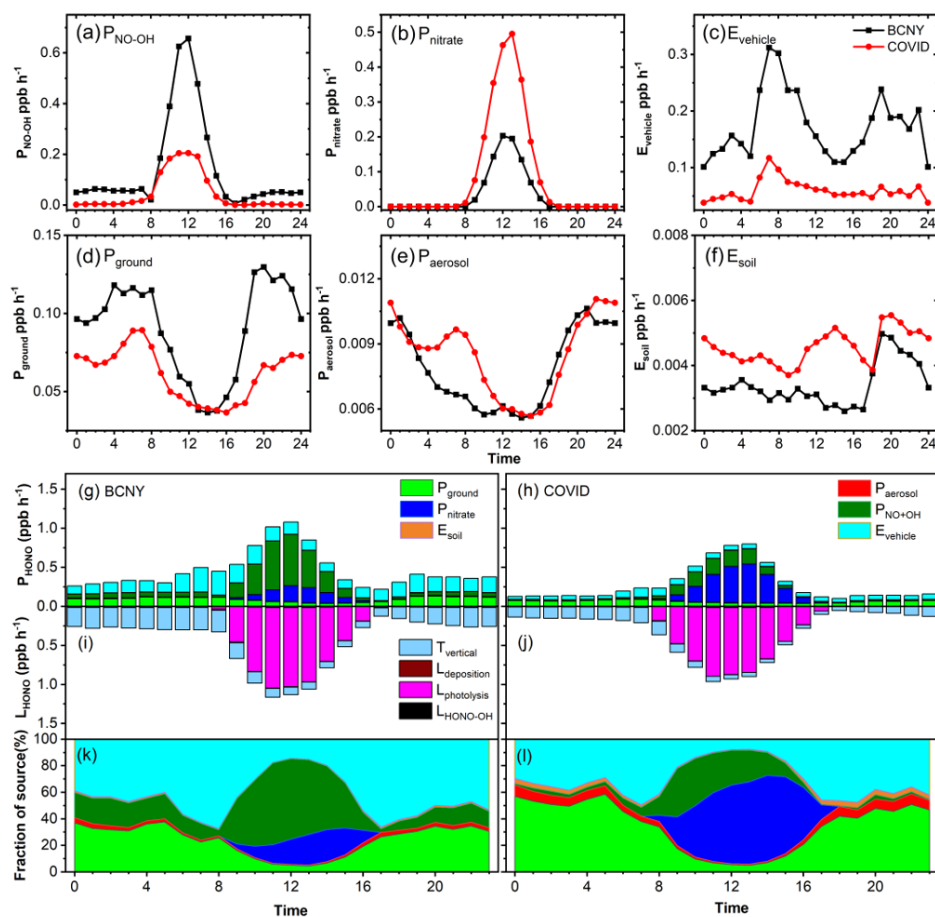
413 the P2 stage, the variation of HONO/NO₂ is different from that of the P1. The HONO/NO₂ in
414 the P2 period was higher than that in the P1 stage, especially in the daytime, although the values
415 of HONO/NO₂ in both stages (P1: 0.036 ± 0.016 ; P2: 0.041 ± 0.038) were lower than that
416 ($0.052\text{-}0.080$) reported by Cui et al (Cui et al., 2018). Subsequently, we further analyzed
417 HONO_{corr}/NO₂ (details shown in Sect. 2.2). The HONO_{corr}/NO₂ attributed to secondary
418 formation via heterogeneous reactions changed obviously after subtracting the interference of
419 other HONO sources. As shown in Fig. S3, the daytime peak of HONO_{corr}/NO₂ in P2 became
420 more prominent compared with that in Fig. 3e. At the same time, the HONO_{corr}/NO₂ ($0.038 \pm$
421 0.035) in P1 was slightly lower than that in P2 (0.042 ± 0.034). However, the HONO
422 concentration decreased significantly as discussed above. These results suggest that
423 heterogeneous reactions of NO₂ on the aerosol surfaces may not be a major source of HONO
424 because the enhanced potential of heterogeneous reactions indicated by PM_{2.5}×NO₂ and
425 HONO_{corr}/NO₂ in P2 contrast with the decreased HONO concentrations compared to P1. In
426 summary, we propose that during our observation period, heterogeneous reactions of NO₂
427 should have a relatively minor contribution to HONO production.

428 **3.3 Relative change of different sources to HONO budget in Beijing during different** 429 **periods.**

430 Figure 4a-f shows the diurnal variation of HONO production or emission rates for these sources
431 at different stages, and Fig. 4g-l shows the budget of the HONO sources and sinks during P1
432 (BCNY) and P2 (COVID-19 lockdown). The HONO production rate via homogeneous
433 reaction between NO and OH in the P1 period was much higher than that in the P2 period,
434 especially during the daytime. The average rate decreased from 0.145 ± 0.189 ppb h⁻¹ in the P1



435 stage to 0.047 ± 0.073 ppb h^{-1} in the P2 stage. The OH concentrations increased slightly from
436 P1 ($4.1 \times 10^5 \pm 5.8 \times 10^5$ cm^{-3}) to P2 ($6.7 \times 10^5 \pm 1.0 \times 10^6$ cm^{-3}). Therefore, the observed decrease
437 in HONO production rate via homogeneous reaction between NO and OH should be ascribed
438 to the substantial reduction of NO concentration as discussed above. It can be seen that the
439 homogeneous reaction between NO and OH is indeed an important source of HONO at night.
440 In previous studies, the nocturnal production of HONO via NO and OH was often ignored
441 because low nighttime OH concentrations were estimated (Fu et al., 2019). However, some
442 studies have shown that the observed nighttime OH concentrations in the Beijing urban area
443 can also be maintained in the order of 10^5 molecules cm^{-3} in winter, which also means that the
444 contribution of the reaction channels of NO and OH to HONO cannot be ignored. In the P1
445 stage, the homogeneous reaction between NO and OH accounted for 13% of the nighttime
446 HONO sources. However, in the daytime, the homogeneous reaction between NO and OH was
447 the most important source of HONO, which accounted for up to 51% of the daytime HONO
448 source. This is consistent with a recent study that proposed the oxidation pathway of NO by
449 OH is the main source of HONO (Song et al., 2023). In the P2 stage, its proportion in the night
450 was negligible due to the dramatic decrease in NO concentration during the pandemic event,
451 and the maximal proportion of HONO sources in the daytime was also reduced to 25%. It is
452 worth noting that the parameterization of OH concentration will introduce uncertainty to
453 HONO sources. Table S2 shows the sensitivity test for the HONO simulation. An increase of
454 10% and 200% in OH concentration in M3 and M4 results in a 24-26% change in the HONO
455 source. It means that the accuracy of the OH measurement is important for understanding the
456 source-sink balance of the HONO.



457

458 **Figure 4.** (a-f): Diurnal variations in HONO production rate from various sources. The black

459 lines are the diurnal curves before CNY and the red ones are during the COVID-19 lockdown.

460 (g-l): Variations of HONO budget. (g,h) Diurnal production rates of HONO; (i,j) loss rates of

461 HONO (unit: ppb h^{-1}); (k,l) relative contributions of each source. Panels (g),(i), and (k) show

462 the data from BCNY, and panels (h),(j), and (l) show the data from the COVID-19 lockdown.

463

464 The daytime HONO source related to photolysis of nitrate ($0.223 \pm 0.175 \text{ ppb h}^{-1}$) in the

465 P2 stage was much larger than that ($0.107 \pm 0.068 \text{ ppb h}^{-1}$) in the P1 stage. It contributed 16%



466 to the daytime HONO source in the P1 period. However, it became the most important daytime
467 source of HONO in the P2 stage, accounting for up to 53%, as both the nitrate concentration
468 and the light intensity increased significantly. Ye et al. (Ye et al., 2016) reported that the
469 photolysis rate constants of nitrate particles on the surface of different materials were in the
470 range of 6.0×10^{-6} - $3.7 \times 10^{-4} \text{ s}^{-1}$. Thus, we used the lower limit value of $6.0 \times 10^{-6} \text{ s}^{-1}$ and the
471 upper limit value of $3.7 \times 10^{-4} \text{ s}^{-1}$ for sensitivity tests (methods M9 and M10), which resulted in
472 a change of 25% and 95% of HONO sources, respectively. The yield of soil emissions in the
473 P2 stage is also higher than that in the P1 stage due to the temperature rise in the P2 stage
474 because the temperature will affect the soil emission flux (Oswald et al., 2013), while the
475 importance of this source is negligible in this study. In M15 and M16, we amplify and shrink
476 the soil emission flux by 10 times, respectively, and the change of the simulated HONO sources
477 was less than 5%.

478 The direct emission rate of HONO from vehicles in the P1 stage was much higher than
479 that in the P2 stage. The emission rate of the P1 stage was between 0.135-0.39 ppb h^{-1} , with a
480 mean value of $0.227 \pm 0.071 \text{ ppb h}^{-1}$. This is comparable with the value (0.079-0.32 ppb h^{-1}) in
481 the winter of 2018 (Liu et al., 2020d). In the P2 stage, it decreased to 0.062-0.173 ppb h^{-1} , with
482 a mean value of $0.086 \pm 0.027 \text{ ppb h}^{-1}$. This value is slightly higher than the lower limit of
483 vehicle emissions of 0.013-0.076 ppb h^{-1} estimated using an emission factor of 0.18% in our
484 previous study (Liu et al., 2020d), while it is less than the upper limit reported by Li (Li et al.,
485 2018) in Jinan of 0.13 ± 0.06 - $0.53 \pm 0.23 \text{ ppb h}^{-1}$. During the lockdown, the emission rate of
486 HONO from vehicles was reduced by 53%-66% when compared with that before the lockdown.
487 In the P1 period, vehicle emission was an important nighttime source of HONO. It contributed



488 53% to the HONO sources, much higher than heterogeneous reactions of NO₂ on aerosol and
489 ground surfaces (33%) (Fig. S7). In the P2 stage, due to the reduction of transport, the
490 contribution of vehicle emissions to HONO sources decreased to 40%, while the contribution
491 of heterogeneous reactions of NO₂ increased to 53%. This is consistent with the observed
492 decrease in HONO concentrations. The daytime contributions of vehicle emissions to HONO
493 sources were lower than the corresponding nighttime contributions, while it was still higher in
494 the P1 period than in the P2 period. These results mean that vehicles should be important
495 contributors to ambient HONO under typical emission patterns in Beijing. In the sensitivity
496 analysis, the emission factors of 0.008 and 0.0186 were considered in methods M1 and M2,
497 and 8% and 20% changes were found in the simulated HONO sources, respectively.

498 As shown in Fig. 4e, the heterogeneous reaction rate of NO₂ on aerosols did not change
499 much between the P1 and P2 stages. The average production rate of HONO in the P1 stage was
500 0.007 ± 0.002 ppb h⁻¹, and it was 0.008 ± 0.002 ppb h⁻¹ in the P2 stage, showing an increase of
501 about 14%. It is worth noting that the HONO formation rate from the heterogeneous conversion
502 of NO₂ on the surface of aerosol does not decrease, which is caused by the increase in PM_{2.5}
503 concentration along with a slight decrease in NO₂ concentration during the P2 period. If the
504 heterogeneous transformation of NO₂ on particulate surfaces is important, especially in the case
505 of heavy pollution, increased HONO concentrations should be expected instead of a large
506 decrease, as observed in the P2 stage. This is consistent with the changes in HONO_{corr}/NO₂ and
507 PM_{2.5}×NO₂ as discussed in Sect. 3.2. For the heterogeneous transformation of NO₂ on the
508 ground and aerosol surfaces, this source is sensitive to the uptake coefficient (γ) of NO₂. Here
509 we assume that the upper limit of γ is 10⁻⁵ (M7) and the lower limit is 2×10⁻⁷ (M8) (Liu et al.,



510 2019b; Liu et al., 2020d). As shown in Table S2, the change in simulated HONO is less than
511 5%. We reduced and magnified the surface area concentration (A_s) of particulate matter by a
512 factor of 10 in M11 and M12, respectively, and the resulting change in HONO was still less
513 than 10%, which also verifies that the heterogeneous reaction of NO_2 on aerosol surfaces may
514 be an unimportant HONO source.

515 Regarding the heterogeneous reaction of NO_2 on ground surfaces, the average formation
516 rate of HONO in the P1 stage was $0.09 \pm 0.03 \text{ ppb h}^{-1}$, while it was $0.06 \pm 0.02 \text{ ppb h}^{-1}$ in the
517 P2 stage. This is ascribed to the significant drop in NO_2 concentration during the COVID-19
518 lockdown. Fig. 4k shows that the heterogeneous reaction of NO_2 on ground surfaces is also an
519 important nighttime source of HONO. In the P1 stage, heterogeneous reactions on both aerosol
520 and ground surfaces explained 33% of the nighttime HONO source. In the daytime, however,
521 the contribution of heterogeneous reactions to HONO sources dropped rapidly. In the P2 stage,
522 the heterogeneous reaction became the most important nighttime source contributing up to 53%
523 of HONO (Fig. S7). This can be explained by the significant decrease in NO and direct
524 emissions of HONO from traffic. Similar to heterogeneous reactions on aerosol surfaces, we
525 assumed that the upper limit of γ_{NO_2} on ground surfaces was 10^{-5} (M5) and the lower limit
526 was 2×10^{-7} (M6), respectively, and the changes in simulated HONO source were 40% and 9%,
527 respectively. In M13 and M14, we set the surface roughness (δ) to 1 and 2.2 as reported in the
528 literature, respectively (Zhang et al., 2022b; Liu et al., 2020c), and the simulated changes in
529 HONO were less than 8%.

530 During the P1 and P2 periods, the mean values of T_{vertical} were $0.195 \pm 0.076 \text{ ppb h}^{-1}$ and
531 $0.102 \pm 0.048 \text{ ppb h}^{-1}$, respectively. It was the main sink of HONO at night. The mean $L_{\text{photolysis}}$



532 was 0.563 ± 0.375 ppb h^{-1} and 0.442 ± 0.324 ppb h^{-1} , respectively, which was the main daytime
533 sink of HONO. The average loss rate of $L_{\text{HONO-OH}}$ during P1 and P2 was 0.005 ppb h^{-1} and
534 0.004 ppb h^{-1} , respectively. The $L_{\text{deposition}}$ was 0.009 ± 0.005 ppb h^{-1} during P1, while it was
535 0.004 ± 0.003 ppb h^{-1} during P2. In M17 and M18, we set the lower limit of the deposition rate
536 (V_d) to 0.00077 and the upper limit to 0.025 (Zhang et al., 2023b), causing a change of 1% and
537 24% in the simulated HONO, respectively. In M19 and M20 at the same time, we set the
538 dilution rate (K_{dilution}) to 0.1 and 0.44, resulting in a 12% and 19% change, respectively.

539 To verify these calculated sources and sinks of HONO, we further estimated the HONO
540 concentration according to Eq. (2) and the parameters described in Sect. 2.2. Fig. S4 shows the
541 time series of estimated HONO concentrations. The observed HONO concentrations were also
542 shown for comparison. The estimated HONO concentrations were well correlated with the
543 observed values from the perspective of both diurnal curves and the scattering point plot during
544 the whole period (Fig. S5 and Fig. S6) although the estimated HONO concentrations were
545 slightly lower than the observed values at noon as shown in Fig. S5. This means that our
546 parametric scheme is overall reasonable but still underestimates the daytime HONO source due
547 to some unknown daytime sources. This unknown source may be related to the photochemical
548 reactions related to NO_2 and nitroaromatic compounds mentioned in recent studies (Liu et al.,
549 2020a). Liu et al. have found the photoenhanced effect of the conversion from NO_2 to HONO
550 on real urban grime and glass windows simulated in laboratory studies (Liu et al., 2019a; Liu
551 et al., 2020b). Yang et al. also have proposed that photolysis of nitroaromatic compounds may
552 be a daytime source of HONO (Yang et al., 2021). Considering the uncertainty of
553 parameterization, we used Oracle Crystal Ball (version 11.1.2.4, Oracle's software for



554 modeling, prediction, simulation, and optimization) (Rahmani et al., 2023) to evaluate the
555 overall uncertainty of the parameterization through Monte Carlo simulations. The relative
556 standard deviation is 27.2% for the HONO budget.

557 In summary, heterogeneous reactions of NO₂ (including ground and aerosol surfaces)
558 contributed 33% to the nocturnal HONO sources in the P1 stage, while they increased to 53%
559 in the P2 stage. Ground surfaces were the main interfaces for heterogeneous reactions,
560 compared to aerosol surfaces. At the same time, vehicle emissions account for 53% and 40%
561 of nighttime HONO sources in the P1 and P2 stages, respectively. Therefore, we can conclude
562 that traffic-related emissions, rather than heterogeneous reactions of NO₂ were the main HONO
563 source at night in Beijing in the typical emission patterns of air pollutants.

564 **4. Conclusions and atmospheric implications.**

565 During the COVID-19 pandemic at the beginning of 2020, the concentration of many air
566 pollutants decreased significantly due to the emission reduction of factories and transportation.
567 The average concentration of NO_x decreased by about 57%, of which NO decreased by about
568 87%, and NO₂ decreased by about 36%. The average concentration of HONO decreased by
569 about 45.3% compared with those before the pandemic control. The average concentration of
570 O₃ and PM_{2.5} increased by approximately 75% and 50%, respectively.

571 In this study, the parameters of HONO sources were optimized. The balance of sources
572 and sinks is well supported by a relatively high correlation between observed and estimated
573 HONO concentrations. During the observation period, we used lockdown during COVID-19
574 as a disturbance factor and compared the concentration and source changes of HONO before
575 and during COVID-19 lockdown to determine whether heterogeneous reactions on the surface



576 of particulate matter and vehicle emissions were important HONO sources. We found that
577 vehicle-related emissions were the most important nighttime HONO source in Beijing,
578 contributing 50-60% to the nighttime HONO sources. The homogeneous reaction between NO
579 and OH and the heterogeneous reaction of NO₂ on the aerosol surface were not important for
580 the contribution of nocturnal HONO, accounting for 13% and 2%, respectively. The
581 heterogeneous reaction of NO₂ on ground surfaces was also found to be an important source of
582 HONO at night, accounting for 31% of the nighttime HONO sources. Nitrate photolysis
583 became the most important source of HONO during the daytime compared with the situation
584 before the pandemic control because of the combined effect of the increase in the average
585 concentration of nitrate and the decrease in the NO concentration during the pandemic. This
586 study confirms that reducing anthropogenic emissions can indeed reduce the concentration of
587 HONO in the atmosphere. However, such reduction does not have a simple linear relation with
588 the reduction in human activities, but it also depends on meteorological conditions and complex
589 chemical transformation processes taking place in the atmosphere.

590 As a megacity in China, Beijing has a large population and intensive traffic emissions, as
591 a result of frequent air pollution. Although concentrations of HONO are usually lower than
592 those of other major pollutants, HONO efficiently triggers the formation of secondary
593 pollutants acting as an important primary source of OH radicals. Therefore, the sources of
594 HONO deserve to be investigated for air pollution control in Beijing. Our results suggest that
595 motor vehicle emissions are an important HONO source, while the contribution of the
596 heterogeneous conversion of NO₂ to HONO on the aerosol surfaces still needs to be further
597 evaluated and, especially, the kinetic parameters on ambient aerosol should be determined. In



598 future research, it is necessary to combine field observations, laboratory studies, and model
599 simulations to quantify the contribution of traffic-related emissions to HONO, and finally
600 obtain an accurate budget of HONO.



601 **Author contributions:** YZ contributed to the methodology, data curation, and writing of the
602 original draft. ZF and FZ contributed to the methodology, investigation, and data curation. CL
603 contributed to methodology, investigation, and data curation. WW contributed to the
604 conceptualization, investigation, reviewing, and editing the text, and supervision. XF
605 contributed to the methodology, reviewing, and editing the text. YZ and WM contributed to the
606 methodology, investigation, data curation, and reviewing and editing the text. ZL and CL
607 contributed to methodology, investigation, and data curation. GZ contributed to the
608 methodology, investigation, resources, and data curation. CY contributed to the methodology,
609 data curation, reviewing, and editing the text. VK, FB, TP, and JK contributed to the acquisition
610 of resources and reviewing and editing the text. MK contributed to the methodology and
611 reviewed the text. YL contributed to the conceptualization, investigation, data curation, writing,
612 reviewing & editing, supervision, and funding acquisition;

613 **Competing interests:** At least one of the (co-)authors is a member of the editorial board of
614 Atmospheric Chemistry and Physics.

615 **Data availability:** Data are available upon request to Yongchun Liu (liuyc@buct.edu.cn).

616 **Acknowledgments:** This research was financially supported by the Beijing Natural Science
617 Foundation (8232041), Beijing National Laboratory for Molecular Sciences (BNLMS-CXXM-
618 202011), and the National Natural Science Foundation of China (42275117 and 41931287).
619 This research was supported in part by Hebei Technological Innovation Center for Volatile
620 Organic Compounds Detection and Treatment in Chemical Industry (ZXJJ20220406) and the
621 Natural Science Foundation of Hebei Province (D2023209012). The work is partially
622 supported by Academy of Finland Flagship “Atmosphere and Climate Competence Center



623 (ACCC), project number 337549 and European Union’s Horizon 2020 research and innovation
624 programme under grant agreement No 101036245 (RI-URBANS) and 101056783 (FOCI) as
625 well as Technology Industries of Finland Centennial Foundation via project “urbaani
626 ilmanlaatu 2.0”.



627 References

- 628 Acker, K., Febo, A., Trick, S., Perrino, C., Bruno, P., Wiesen, P., Möller, D., Wieprecht, W., Auel, R., Giusto, M.,
629 Geyer, A., Platt, U., and Allegrini, I.: Nitrous acid in the urban area of Rome, *Atmospheric Environment*, 40, 3123-
630 3133, 10.1016/j.atmosenv.2006.01.028, 2006.
- 631 Alicke, B.: Impact of nitrous acid photolysis on the total hydroxyl radical budget during the Limitation of Oxidant
632 Production/Pianura Padana Produzione di Ozono study in Milan, *Journal of Geophysical Research*, 107,
633 10.1029/2000jd000075, 2002.
- 634 Chen, Y., Wang, W., Lian, C., Peng, C., Zhang, W., Li, J., Liu, M., Shi, B., Wang, X., and Ge, M.: Evaluation and
635 impact factors of indoor and outdoor gas-phase nitrous acid under different environmental conditions, *J Environ*
636 *Sci (China)*, 95, 165-171, 10.1016/j.jes.2020.03.048, 2020.
- 637 Crilley, L. R., Kramer, L. J., Ouyang, B., Duan, J., Zhang, W., Tong, S., Ge, M., Tang, K., Qin, M., Xie, P., Shaw,
638 M. D., Lewis, A. C., Mehra, A., Bannan, T. J., Worrall, S. D., Priestley, M., Bacak, A., Coe, H., Allan, J., Percival,
639 C. J., Popoola, O. A. M., Jones, R. L., and Bloss, W. J.: Intercomparison of nitrous acid (HONO) measurement
640 techniques in a megacity (Beijing), *Atmos. Meas. Tech.*, 12, 6449-6463, 10.5194/amt-12-6449-2019, 2019.
- 641 Cui, L., Li, R., Zhang, Y., Meng, Y., Fu, H., and Chen, J.: An observational study of nitrous acid (HONO) in
642 Shanghai, China: The aerosol impact on HONO formation during the haze episodes, *Sci Total Environ*, 630, 1057-
643 1070, 10.1016/j.scitotenv.2018.02.063, 2018.
- 644 Cui, Y., Ji, D., Maenhaut, W., Gao, W., Zhang, R., and Wang, Y.: Levels and sources of hourly PM_{2.5}-related
645 elements during the control period of the COVID-19 pandemic at a rural site between Beijing and Tianjin, *Sci*
646 *Total Environ*, 744, 140840, 10.1016/j.scitotenv.2020.140840, 2020.
- 647 Dillon, M. B., Lamanna, M. S., Schade, G. W., Goldstein, A. H., and Cohen, R. C.: Chemical evolution of the
648 Sacramento urban plume: Transport and oxidation, *Journal of Geophysical Research: Atmospheres*, 107, ACH 3-
649 1-ACH 3-15, 10.1029/2001jd000969, 2002.
- 650 Ehhalt, D. H. and Rohrer, F.: Dependence of the OH concentration on solar UV, *Journal of Geophysical Research:*
651 *Atmospheres*, 105, 3565-3571, 10.1029/1999jd901070, 2000.
- 652 Farren, N. J., Ramirez, N., Lee, J. D., Finessi, E., Lewis, A. C., and Hamilton, J. F.: Estimated Exposure Risks
653 from Carcinogenic Nitrosamines in Urban Airborne Particulate Matter, *Environ Sci Technol*, 49, 9648-9656,
654 10.1021/acs.est.5b01620, 2015.
- 655 Fu, X., Wang, T., Zhang, L., Li, Q., Wang, Z., Xia, M., Yun, H., Wang, W., Yu, C., Yue, D., Zhou, Y., Zheng, J.,
656 and Han, R.: The significant contribution of HONO to secondary pollutants during a severe winter pollution event
657 in southern China, *Atmospheric Chemistry and Physics*, 19, 1-14, 10.5194/acp-19-1-2019, 2019.
- 658 Ge, S., Wang, G., Zhang, S., Li, D., Xie, Y., Wu, C., Yuan, Q., Chen, J., and Zhang, H.: Abundant NH₃ in China
659 Enhances Atmospheric HONO Production by Promoting the Heterogeneous Reaction of SO₂ with NO₂, *Environ*
660 *Sci Technol*, 53, 14339-14347, 10.1021/acs.est.9b04196, 2019.
- 661 Han, C., Liu, Y., and He, H.: Role of organic carbon in heterogeneous reaction of NO₂ with soot, *Environ Sci*
662 *Technol*, 47, 3174-3181, 10.1021/es304468n, 2013.
- 663 Han, C., Liu, Y., and He, H.: Heterogeneous reaction of NO₂ with soot at different relative humidity, *Environ Sci*
664 *Pollut Res Int*, 24, 21248-21255, 10.1007/s11356-017-9766-y, 2017a.
- 665 Han, C., Yang, W., Wu, Q., Yang, H., and Xue, X.: Heterogeneous Photochemical Conversion of NO₂ to HONO
666 on the Humic Acid Surface under Simulated Sunlight, *Environ Sci Technol*, 50, 5017-5023,
667 10.1021/acs.est.5b05101, 2016.
- 668 Han, X., Zhang, M., Skorokhod, A., and Kou, X.: Modeling dry deposition of reactive nitrogen in China with
669 RAMS-CMAQ, *Atmospheric Environment*, 166, 47-61, 10.1016/j.atmosenv.2017.07.015, 2017b.



- 670 Hao, Q., Jiang, N., Zhang, R., Yang, L., and Li, S.: Characteristics, sources and reactions of nitrous acid during
671 winter in the core city of the Central Plains Economic Region in China via high-time-resolution online,
672 Atmospheric Chemistry and Physics Discussions, 10.5194/acp-2019-916, 2019.
- 673 Huang, R. J., Yang, L., Cao, J., Wang, Q., Tie, X., Ho, K. F., Shen, Z., Zhang, R., Li, G., Zhu, C., Zhang, N., Dai,
674 W., Zhou, J., Liu, S., Chen, Y., Chen, J., and O'Dowd, C. D.: Concentration and sources of atmospheric nitrous
675 acid (HONO) at an urban site in Western China, *Sci Total Environ*, 593-594, 165-172,
676 10.1016/j.scitotenv.2017.02.166, 2017.
- 677 Jiang, Y., Xue, L., Shen, H., Dong, C., Xiao, Z., and Wang, W.: Dominant Processes of HONO Derived from
678 Multiple Field Observations in Contrasting Environments, *Environmental Science & Technology Letters*, 9, 258-
679 264, 10.1021/acs.estlett.2c00004, 2022.
- 680 Kanaya, Y., Cao, R., Akimoto, H., Fukuda, M., Komazaki, Y., Yokouchi, Y., Koike, M., Tanimoto, H., Takegawa,
681 N., and Kondo, Y.: Urban photochemistry in central Tokyo: 1. Observed and modeled OH and HO₂ radical
682 concentrations during the winter and summer of 2004, *Journal of Geophysical Research*, 112,
683 10.1029/2007jd008670, 2007.
- 684 Kim, M. and Or, D.: Microscale pH variations during drying of soils and desert biocrusts affect HONO and NH₃
685 emissions, *Nat Commun*, 10, 3944, 10.1038/s41467-019-11956-6, 2019.
- 686 Kramer, L. J., Crilley, L. R., Adams, T. J., Ball, S. M., Pope, F. D., and Bloss, W. J.: Nitrous acid (HONO)
687 emissions under real-world driving conditions from vehicles in a UK road tunnel, *Atmospheric Chemistry and
688 Physics*, 20, 5231-5248, 10.5194/acp-20-5231-2020, 2020.
- 689 Kroll, J. H., Heald, C. L., Cappa, C. D., Farmer, D. K., Fry, J. L., Murphy, J. G., and Steiner, A. L.: The complex
690 chemical effects of COVID-19 shutdowns on air quality, *Nat Chem*, 12, 777-779, 10.1038/s41557-020-0535-z,
691 2020.
- 692 Kulmala, M. and Petäjä, T.: Soil Nitrites Influence Atmospheric Chemistry, *Science* 333, 1586-1587, 2011.
- 693 Le, T., Wang, Y., Liu, L., Yang, J., Yung, Y. L., Li, G., and Seinfeld, J. H.: Unexpected air pollution with marked
694 emission reductions during the COVID-19 outbreak in China, *Science*, 369, 702+, 10.1126/science.abb7431,
695 2020.
- 696 Li, D., Xue, L., Wen, L., Wang, X., Chen, T., Mellouki, A., Chen, J., and Wang, W.: Characteristics and sources
697 of nitrous acid in an urban atmosphere of northern China: Results from 1-yr continuous observations, *Atmospheric
698 Environment*, 182, 296-306, 10.1016/j.atmosenv.2018.03.033, 2018.
- 699 Li, S., Song, W., Zhan, H., Zhang, Y., Zhang, X., Li, W., Tong, S., Pei, C., Wang, Y., Chen, Y., Huang, Z., Zhang,
700 R., Zhu, M., Fang, H., Wu, Z., Wang, J., Luo, S., Fu, X., Xiao, S., Huang, X., Zeng, J., Zhang, H., Chen, D.,
701 Gligorovski, S., Ge, M., George, C., and Wang, X.: Contribution of Vehicle Emission and NO₂ Surface
702 Conversion to Nitrous Acid (HONO) in Urban Environments: Implications from Tests in a Tunnel, *Environ Sci
703 Technol*, 10.1021/acs.est.1c00405, 2021.
- 704 Li, X., Brauers, T., Häseler, R., Bohn, B., Fuchs, H., Hofzumahaus, A., Holland, F., Lou, S., Lu, K. D., Rohrer, F.,
705 Hu, M., Zeng, L. M., Zhang, Y. H., Garland, R. M., Su, H., Nowak, A., Wiedensohler, A., Takegawa, N., Shao,
706 M., and Wahner, A.: Exploring the atmospheric chemistry of nitrous acid (HONO) at a rural site in Southern China,
707 *Atmospheric Chemistry and Physics*, 12, 1497-1513, 10.5194/acp-12-1497-2012, 2012.
- 708 Liang, Y., Zha, Q., Wang, W., Cui, L., Lui, K. H., Ho, K. F., Wang, Z., Lee, S. C., and Wang, T.: Revisiting nitrous
709 acid (HONO) emission from on-road vehicles: A tunnel study with a mixed fleet, *J Air Waste Manag Assoc*, 67,
710 797-805, 10.1080/10962247.2017.1293573, 2017.
- 711 Liao, S., Zhang, J., Yu, F., Zhu, M., Liu, J., Ou, J., Dong, H., Sha, Q., Zhong, Z., Xie, Y., Luo, H., Zhang, L., and
712 Zheng, J.: High Gaseous Nitrous Acid (HONO) Emissions from Light-Duty Diesel Vehicles, *Environ Sci Technol*,
713 55, 200-208, 10.1021/acs.est.0c05599, 2021.



- 714 Liu, J., Deng, H., Lakey, P. S. J., Jiang, H., Mekic, M., Wang, X., Shiraiwa, M., and Gligorovski, S.: Unexpectedly
715 High Indoor HONO Concentrations Associated with Photochemical NO₂ Transformation on Glass Windows,
716 *Environmental Science & Technology*, 54, 15680-15688, 10.1021/acs.est.0c05624, 2020a.
- 717 Liu, J., Li, S., Mekic, M., Jiang, H., Zhou, W., Loisel, G., Song, W., Wang, X., and Gligorovski, S.: Photoenhanced
718 Uptake of NO₂ and HONO Formation on Real Urban Grime, *Environmental Science & Technology Letters*, 6,
719 413-417, 10.1021/acs.estlett.9b00308, 2019a.
- 720 Liu, J., Deng, H., Li, S., Jiang, H., Mekic, M., Zhou, W., Wang, Y., Loisel, G., Wang, X., and Gligorovski, S.:
721 Light-enhanced heterogeneous conversion of NO₂ to HONO on solid films consisted of fluorene and
722 fluorene/Na₂SO₄: An impact on urban and indoor atmosphere, *Environ Sci Technol*, 10.1021/acs.est.0c02627,
723 2020b.
- 724 Liu, Y., Han, C., Ma, J., Bao, X., and He, H.: Influence of relative humidity on heterogeneous kinetics of NO₂ on
725 kaolin and hematite, *Phys Chem Chem Phys*, 17, 19424-19431, 10.1039/c5cp02223a, 2015.
- 726 Liu, Y., Nie, W., Xu, Z., Wang, T., Wang, R., Li, Y., Wang, L., Chi, X., and Ding, A.: Semi-quantitative
727 understanding of source contribution to nitrous acid (HONO) based on 1 year of continuous observation at the
728 SORPES station in eastern China, *Atmospheric Chemistry and Physics*, 19, 13289-13308, 10.5194/acp-19-13289-
729 2019, 2019b.
- 730 Liu, Y., Ni, S., Jiang, T., Xing, S., Zhang, Y., Bao, X., Feng, Z., Fan, X., Zhang, L., and Feng, H.: Influence of
731 Chinese New Year overlapping COVID-19 lockdown on HONO sources in Shijiazhuang, *Sci Total Environ*, 745,
732 141025, 10.1016/j.scitotenv.2020.141025, 2020c.
- 733 Liu, Y., Lu, K., Li, X., Dong, H., Tan, Z., Wang, H., Zou, Q., Wu, Y., Zeng, L., Hu, M., Min, K. E., Kecorius, S.,
734 Wiedensohler, A., and Zhang, Y.: A Comprehensive Model Test of the HONO Sources Constrained to Field
735 Measurements at Rural North China Plain, *Environ Sci Technol*, 53, 3517-3525, 10.1021/acs.est.8b06367, 2019c.
- 736 Liu, Y., Zhang, Y., Lian, C., Yan, C., Feng, Z., Zheng, F., Fan, X., Chen, Y., Wang, W., Chu, B., Wang, Y., Cai, J.,
737 Du, W., Daellenbach, K. R., Kangasluoma, J., Bianchi, F., Kujansuu, J., Petäjä, T., Wang, X., Hu, B., Wang, Y.,
738 Ge, M., He, H., and Kulmala, M.: The promotion effect of nitrous acid on aerosol formation in wintertime in
739 Beijing: the possible contribution of traffic-related emissions, *Atmospheric Chemistry and Physics*, 20, 13023-
740 13040, 10.5194/acp-20-13023-2020, 2020d.
- 741 Liu, Z., Wang, Y., Costabile, F., Amoroso, A., Zhao, C., Huey, L. G., Stickel, R., Liao, J., and Zhu, T.: Evidence
742 of aerosols as a media for rapid daytime HONO production over China, *Environ Sci Technol*, 48, 14386-14391,
743 10.1021/es504163z, 2014.
- 744 Lv, Z., Wang, X., Deng, F., Ying, Q., Archibald, A. T., Jones, R. L., Ding, Y., Cheng, Y., Fu, M., Liu, Y., Man, H.,
745 Xue, Z., He, K., Hao, J., and Liu, H.: Source-Receptor Relationship Revealed by the Halted Traffic and
746 Aggravated Haze in Beijing during the COVID-19 Lockdown, *Environ Sci Technol*, 54, 15660-15670,
747 10.1021/acs.est.0c04941, 2020.
- 748 Ma, X., Tan, Z., Lu, K., Yang, X., Liu, Y., Li, S., Li, X., Chen, S., Novelli, A., Cho, C., Zeng, L., Wahner, A., and
749 Zhang, Y.: Winter photochemistry in Beijing: Observation and model simulation of OH and HO₂ radicals at an
750 urban site, *Sci Total Environ*, 685, 85-95, 10.1016/j.scitotenv.2019.05.329, 2019.
- 751 Meng, F., Qin, M., Tang, K., Duan, J., Fang, W., Liang, S., Ye, K., Xie, P., Sun, Y., Xie, C., Ye, C., Fu, P., Liu, J.,
752 and Liu, W.: High-resolution vertical distribution and sources of HONO and NO₂ in the nocturnal boundary layer
753 in urban Beijing, China, *Atmospheric Chemistry and Physics*, 20, 5071-5092, 10.5194/acp-20-5071-2020, 2020.
- 754 Nie, W., Ding, A. J., Xie, Y. N., Xu, Z., Mao, H., Kerminen, V. M., Zheng, L. F., Qi, X. M., Huang, X., Yang, X.
755 Q., Sun, J. N., Herrmann, E., Petäjä, T., Kulmala, M., and Fu, C. B.: Influence of biomass burning plumes on
756 HONO chemistry in eastern China, *Atmospheric Chemistry and Physics*, 15, 1147-1159, 10.5194/acp-15-1147-
757 2015, 2015.



- 758 Oswald, R., Behrendt, T., Ermel, M., Wu, D., Su, H., Cheng, Y., Breuninger, C., Moravek, A., Mouglin, E., Delon,
759 C., Loubet, B., Pommerening-Roser, A., Sorgel, M., Poschl, U., Hoffmann, T., Andreae, M. O., Meixner, F. X.,
760 and Trebs, I.: HONO emissions from soil bacteria as a major source of atmospheric reactive nitrogen, *Science*,
761 341, 1233-1235, 10.1126/science.1242266, 2013.
- 762 Pusede, S. E., VandenBoer, T. C., Murphy, J. G., Markovic, M. Z., Young, C. J., Veres, P. R., Roberts, J. M.,
763 Washenfelder, R. A., Brown, S. S., Ren, X., Tsai, C., Stutz, J., Brune, W. H., Browne, E. C., Wooldridge, P. J.,
764 Graham, A. R., Weber, R., Goldstein, A. H., Dusanter, S., Griffith, S. M., Stevens, P. S., Lefer, B. L., and Cohen,
765 R. C.: An Atmospheric Constraint on the NO₂ Dependence of Daytime Near-Surface Nitrous Acid (HONO),
766 *Environ Sci Technol*, 49, 12774-12781, 10.1021/acs.est.5b02511, 2015.
- 767 Qin, M., Xie, P., Su, H., Gu, J., Peng, F., Li, S., Zeng, L., Liu, J., Liu, W., and Zhang, Y.: An observational study
768 of the HONO–NO₂ coupling at an urban site in Guangzhou City, South China, *Atmospheric Environment*, 43,
769 5731-5742, 10.1016/j.atmosenv.2009.08.017, 2009.
- 770 R. Kurtenbach, K.H. Becker, J.A.G. Gomes, J. Kleffmann, J.C. Lörzer, M. Spittler, P. Wiesen, R. Ackermann, A.
771 Geyer, and Platt, U.: Investigations of emissions and heterogeneous formation of HONO in a road traffic tunnel,
772 *Atmospheric Environment*, , 3385–3394, 2001.
- 773 Rahmani, A., Khamutian, S., Doosti-Irani, A., Saatchi, O., and Shokoohizadeh, M. J.: Arsenic level in drinking
774 water, its correlation with water quality parameters, and associated health risks, *Environmental Monitoring and*
775 *Assessment*, 195, 10.1007/s10661-023-11486-1, 2023.
- 776 Shen, N., Zhao, X., Li, L., Zhou, B., Duan, F., and Zhao, W.: Spatial and temporal variation characteristics of
777 atmospheric NO₂ and SO₂ in the Beijing-Tianjin-Hebei region before and after the COVID-19 outbreak, *Air Qual*
778 *Atmos Health*, 1-14, 10.1007/s11869-021-01016-8, 2021.
- 779 Song, M., Zhao, X., Liu, P., Mu, J., He, G., Zhang, C., Tong, S., Xue, C., Zhao, X., Ge, M., and Mu, Y.:
780 Atmospheric NO_x oxidation as major sources for nitrous acid (HONO), *npj Climate and Atmospheric Science*, 6,
781 10.1038/s41612-023-00357-8, 2023.
- 782 Spataro, F., Ianniello, A., Salvatori, R., Nardino, M., Esposito, G., and Montagnoli, M.: Sources of atmospheric
783 nitrous acid (HONO) in the European High Arctic, *Rendiconti Lincei*, 28, 25-33, 10.1007/s12210-016-0568-9,
784 2016.
- 785 Stemmler, K.: Light induced conversion of nitrogen dioxide into nitrous acid on submicron humic acid aerosol,
786 *Atmospheric Chemistry and Physics*, 2007.
- 787 Sun, J., Shen, Z., Zeng, Y., Niu, X., Wang, J., Cao, J., Gong, X., Xu, H., Wang, T., Liu, H., and Yang, L.:
788 Characterization and cytotoxicity of PAHs in PM_{2.5} emitted from residential solid fuel burning in the Guanzhong
789 Plain, China, *Environ Pollut*, 241, 359-368, 10.1016/j.envpol.2018.05.076, 2018.
- 790 Sun, J., Shen, Z., Cao, J., Zhang, L., Wu, T., Zhang, Q., Yin, X., Lei, Y., Huang, Y., Huang, R. J., Liu, S., Han, Y.,
791 Xu, H., Zheng, C., and Liu, P.: Particulate matters emitted from maize straw burning for winter heating in rural
792 areas in Guanzhong Plain, China: Current emission and future reduction, *Atmospheric Research*, 184, 66-76,
793 10.1016/j.atmosres.2016.10.006, 2017.
- 794 Sun, Y., Lei, L., Zhou, W., Chen, C., He, Y., Sun, J., Li, Z., Xu, W., Wang, Q., Ji, D., Fu, P., Wang, Z., and Worsnop,
795 D. R.: A chemical cocktail during the COVID-19 outbreak in Beijing, China: Insights from six-year aerosol
796 particle composition measurements during the Chinese New Year holiday, *Sci Total Environ*, 742, 140739,
797 10.1016/j.scitotenv.2020.140739, 2020.
- 798 Sun, Y. L., Wang, Z. F., Fu, P. Q., Yang, T., Jiang, Q., Dong, H. B., Li, J., and Jia, J. J.: Aerosol composition,
799 sources and processes during wintertime in Beijing, China, *Atmospheric Chemistry and Physics*, 13, 4577-4592,
800 10.5194/acp-13-4577-2013, 2013.
- 801 Tan, Z., Lu, K., Jiang, M., Su, R., Wang, H., Lou, S., Fu, Q., Zhai, C., Tan, Q., Yue, D., Chen, D., Wang, Z., Xie,



- 802 S., Zeng, L., and Zhang, Y.: Daytime atmospheric oxidation capacity in four Chinese megacities during the
803 photochemically polluted season: a case study based on box model simulation, *Atmospheric Chemistry and*
804 *Physics*, 19, 3493-3513, 10.5194/acp-19-3493-2019, 2019.
- 805 Tan, Z., Hofzumahaus, A., Lu, K., Brown, S. S., Holland, F., Huey, L. G., Kiendler-Scharr, A., Li, X., Liu, X., Ma,
806 N., Min, K. E., Rohrer, F., Shao, M., Wahner, A., Wang, Y., Wiedensohler, A., Wu, Y., Wu, Z., Zeng, L., Zhang,
807 Y., and Fuchs, H.: No Evidence for a Significant Impact of Heterogeneous Chemistry on Radical Concentrations
808 in the North China Plain in Summer 2014, *Environ Sci Technol*, 54, 5973-5979, 10.1021/acs.est.0c00525, 2020.
- 809 Tan, Z., Fuchs, H., Lu, K., Hofzumahaus, A., Bohn, B., Broch, S., Dong, H., Gomm, S., Häsel, R., He, L.,
810 Holland, F., Li, X., Liu, Y., Lu, S., Rohrer, F., Shao, M., Wang, B., Wang, M., Wu, Y., Zeng, L., Zhang, Y., Wahner,
811 A., and Zhang, Y.: Radical chemistry at a rural site (Wangdu) in the North China Plain: observation and model
812 calculations of OH, HO₂ and RO₂ radicals, *Atmospheric Chemistry and Physics*, 17, 663-690, 10.5194/acp-17-
813 663-2017, 2017.
- 814 Tan, Z., Rohrer, F., Lu, K., Ma, X., Bohn, B., Broch, S., Dong, H., Fuchs, H., Gkatzelis, G. I., Hofzumahaus, A.,
815 Holland, F., Li, X., Liu, Y., Liu, Y., Novelli, A., Shao, M., Wang, H., Wu, Y., Zeng, L., Hu, M., Kiendler-Scharr,
816 A., Wahner, A., and Zhang, Y.: Wintertime photochemistry in Beijing: observations of RO_x radical concentrations
817 in the North China Plain during the BEST-ONE campaign, *Atmospheric Chemistry and Physics*, 18, 12391-12411,
818 10.5194/acp-18-12391-2018, 2018.
- 819 Tong, S., Hou, S., Zhang, Y., Chu, B., Liu, Y., He, H., Zhao, P., and Ge, M.: Exploring the nitrous acid (HONO)
820 formation mechanism in winter Beijing: direct emissions and heterogeneous production in urban and suburban
821 areas, *Faraday Discuss*, 189, 213-230, 10.1039/c5fd00163c, 2016.
- 822 Wang, J., Xu, X., Wang, S., He, S., Li, X., and He, P.: Heterogeneous effects of COVID-19 lockdown measures
823 on air quality in Northern China, *Appl Energy*, 282, 116179, 10.1016/j.apenergy.2020.116179, 2021.
- 824 Wang, P., Chen, K., Zhu, S., Wang, P., and Zhang, H.: Severe air pollution events not avoided by reduced
825 anthropogenic activities during COVID-19 outbreak, *Resour Conserv Recycl*, 158, 104814,
826 10.1016/j.resconrec.2020.104814, 2020a.
- 827 Wang, S., Zhou, R., Zhao, H., Wang, Z., Chen, L., and Zhou, B.: Long-term observation of atmospheric nitrous
828 acid (HONO) and its implication to local NO₂ levels in Shanghai, China, *Atmospheric Environment*, 77, 718-724,
829 10.1016/j.atmosenv.2013.05.071, 2013.
- 830 Wang, Y., Wen, Y., Wang, Y., Zhang, S., Zhang, K. M., Zheng, H., Xing, J., Wu, Y., and Hao, J.: Four-Month
831 Changes in Air Quality during and after the COVID-19 Lockdown in Six Megacities in China, *Environmental*
832 *Science & Technology Letters*, 7, 802-808, 10.1021/acs.estlett.0c00605, 2020b.
- 833 Weber, B., Wu, D., Tamm, A., Ruckteschler, N., Rodriguez-Caballero, E., Steinkamp, J., Meusel, H., Elbert, W.,
834 Behrendt, T., Sorgel, M., Cheng, Y., Crutzen, P. J., Su, H., and Poschl, U.: Biological soil crusts accelerate the
835 nitrogen cycle through large NO and HONO emissions in drylands, *Proc Natl Acad Sci U S A*, 112, 15384-15389,
836 10.1073/pnas.1515818112, 2015.
- 837 Wu, D., Horn, M. A., Behrendt, T., Muller, S., Li, J., Cole, J. A., Xie, B., Ju, X., Li, G., Ermel, M., Oswald, R.,
838 Frohlich-Nowoisky, J., Hoor, P., Hu, C., Liu, M., Andreae, M. O., Poschl, U., Cheng, Y., Su, H., Trebs, I., Weber,
839 B., and Sorgel, M.: Soil HONO emissions at high moisture content are driven by microbial nitrate reduction to
840 nitrite: tackling the HONO puzzle, *ISME J*, 13, 1688-1699, 10.1038/s41396-019-0379-y, 2019.
- 841 Xu, Z., Wang, T., Wu, J., Xue, L., Chan, J., Zha, Q., Zhou, S., Louie, P. K. K., and Luk, C. W. Y.: Nitrous acid
842 (HONO) in a polluted subtropical atmosphere: Seasonal variability, direct vehicle emissions and heterogeneous
843 production at ground surface, *Atmospheric Environment*, 106, 100-109, 10.1016/j.atmosenv.2015.01.061, 2015.
- 844 Xue, C.: Substantially Growing Interest in the Chemistry of Nitrous Acid (HONO) in China: Current
845 Achievements, Problems, and Future Directions, *Environ Sci Technol*, 10.1021/acs.est.2c02237, 2022.



- 846 Xue, C., Zhang, C., Ye, C., Liu, P., Catoire, V., Krysztofiak, G., Chen, H., Ren, Y., Zhao, X., Wang, J., Zhang, F.,
847 Zhang, C., Zhang, J., An, J., Wang, T., Chen, J., Kleffmann, J., Mellouki, A., and Mu, Y.: HONO Budget and Its
848 Role in Nitrate Formation in the Rural North China Plain, *Environmental Science & Technology*, 54, 11048-11057,
849 10.1021/acs.est.0c01832, 2020.
- 850 Yang, D., Zhang, S., Niu, T., Wang, Y., Xu, H., Zhang, K. M., and Wu, Y.: High-resolution mapping of vehicle
851 emissions of atmospheric pollutants based on large-scale, real-world traffic datasets, *Atmospheric Chemistry and
852 Physics*, 19, 8831-8843, 10.5194/acp-19-8831-2019, 2019.
- 853 Yang, W., You, D., Li, C., Han, C., Tang, N., Yang, H., and Xue, X.: Photolysis of Nitroaromatic Compounds
854 under Sunlight: A Possible Daytime Photochemical Source of Nitrous Acid?, *Environmental Science &
855 Technology Letters*, 8, 747-752, 10.1021/acs.estlett.1c00614, 2021.
- 856 Ye, C., Gao, H., Zhang, N., and Zhou, X.: Photolysis of Nitric Acid and Nitrate on Natural and Artificial Surfaces,
857 *Environ Sci Technol*, 50, 3530-3536, 10.1021/acs.est.5b05032, 2016.
- 858 Yu, Y., Galle, B., Panday, A., Hodson, E., Prinn, R., and Wang, S.: Observations of high rates of NO₂-HONO
859 conversion in the nocturnal atmospheric boundary layer in Kathmandu, Nepal, *Atmospheric Chemistry and
860 Physics*, 6401-6415, 2009.
- 861 Zhang, J., An, J., Qu, Y., Liu, X., and Chen, Y.: Impacts of potential HONO sources on the concentrations of
862 oxidants and secondary organic aerosols in the Beijing-Tianjin-Hebei region of China, *Sci Total Environ*, 647,
863 836-852, 10.1016/j.scitotenv.2018.08.030, 2019a.
- 864 Zhang, J., Chen, J., Xue, C., Chen, H., Zhang, Q., Liu, X., Mu, Y., Guo, Y., Wang, D., Chen, Y., Li, J., Qu, Y., and
865 An, J.: Impacts of six potential HONO sources on HO_x budgets and SOA formation during a wintertime heavy
866 haze period in the North China Plain, *Sci Total Environ*, 681, 110-123, 10.1016/j.scitotenv.2019.05.100, 2019b.
- 867 Zhang, J., Lian, C., Wang, W., Ge, M., Guo, Y., Ran, H., Zhang, Y., Zheng, F., Fan, X., Yan, C., Daellenbach, K.
868 R., Liu, Y., Kulmala, M., and An, J.: Amplified role of potential HONO sources in O₃ formation in North China
869 Plain during autumn haze aggravating processes, *Atmospheric Chemistry and Physics*, 22, 3275-3302,
870 10.5194/acp-22-3275-2022, 2022a.
- 871 Zhang, L., Wang, T., Zhang, Q., Zheng, J., Xu, Z., and Lv, M.: Potential sources of nitrous acid (HONO) and their
872 impacts on ozone: A WRF-Chem study in a polluted subtropical region, *Journal of Geophysical Research:
873 Atmospheres*, 121, 3645-3662, 10.1002/2015jd024468, 2016.
- 874 Zhang, Q., Liu, P., George, C., Chen, T., Ren, Y., Mu, Y., Song, M., Herrmann, H., Mellouki, A., Chen, J., Zhao,
875 X., and Zeng, Y.: Unveiling the underestimated direct emissions of nitrous acid (HONO), *Proceedings of the
876 National Academy of Sciences*, 120, 10.1073/pnas, 2023a.
- 877 Zhang, W., Tong, S., Ge, M., An, J., Shi, Z., Hou, S., Xia, K., Qu, Y., Zhang, H., Chu, B., Sun, Y., and He, H.:
878 Variations and sources of nitrous acid (HONO) during a severe pollution episode in Beijing in winter 2016, *Sci
879 Total Environ*, 648, 253-262, 10.1016/j.scitotenv.2018.08.133, 2019c.
- 880 Zhang, W., Ren, Y., Zhang, C., Liu, P., Xue, C., Ye, C., Liu, C., Wang, J., Zhang, Y., Liu, J., Song, Y., Feng, Y.,
881 and Mu, Y.: Aging of pollution air parcels acts as the dominant source for nocturnal HONO, *Sci Total Environ*,
882 881, 163438, 10.1016/j.scitotenv.2023.163438, 2023b.
- 883 Zhang, W., Tong, S., Jia, C., Wang, L., Liu, B., Tang, G., Ji, D., Hu, B., Liu, Z., Li, W., Wang, Z., Liu, Y., Wang,
884 Y., and Ge, M.: Different HONO Sources for Three Layers at the Urban Area of Beijing, *Environ Sci Technol*, 54,
885 12870-12880, 10.1021/acs.est.0c02146, 2020.
- 886 Zhang, X., Tong, S., Jia, C., Zhang, W., Wang, Z., Tang, G., Hu, B., Liu, Z., Wang, L., Zhao, P., Pan, Y., and Ge,
887 M.: Elucidating HONO formation mechanism and its essential contribution to OH during haze events, *npj Climate
888 and Atmospheric Science*, 6, 10.1038/s41612-023-00371-w, 2023c.
- 889 Zhang, X., Tong, S., Jia, C., Zhang, W., Li, J., Wang, W., Sun, Y., Wang, X., Wang, L., Ji, D., Wang, L., Zhao, P.,



890 Tang, G., Xin, J., Li, A., and Ge, M.: The Levels and Sources of Nitrous Acid (HONO) in Winter of Beijing and
891 Sanmenxia, *Journal of Geophysical Research: Atmospheres*, 127, 10.1029/2021jd036278, 2022b.

892 Zhao, Y., Zhang, K., Xu, X., Shen, H., Zhu, X., Zhang, Y., Hu, Y., and Shen, G.: Substantial Changes in Nitrogen
893 Dioxide and Ozone after Excluding Meteorological Impacts during the COVID-19 Outbreak in Mainland China,
894 *Environmental Science & Technology Letters*, 7, 402-408, 10.1021/acs.estlett.0c00304, 2020.

895 Zheng, B., Huo, H., Zhang, Q., Yao, Z. L., Wang, X. T., Yang, X. F., Liu, H., and He, K. B.: High-resolution
896 mapping of vehicle emissions in China in 2008, *Atmospheric Chemistry and Physics*, 14, 9787-9805, 10.5194/acp-
897 14-9787-2014, 2014.

898 Zheng, J., Shi, X., Ma, Y., Ren, X., Jabbour, H., Diao, Y., Wang, W., Ge, Y., Zhang, Y., and Zhu, W.: Contribution
899 of nitrous acid to the atmospheric oxidation capacity in an industrial zone in the Yangtze River Delta region of
900 China, *Atmospheric Chemistry and Physics*, 20, 5457-5475, 10.5194/acp-20-5457-2020, 2020.

901 Zhou, X., Zhang, N., TerAvest, M., Tang, D., Hou, J., Bertman, S., Alaghmand, M., Shepson, P. B., Carroll, M.
902 A., Griffith, S., Dusanter, S., and Stevens, P. S.: Nitric acid photolysis on forest canopy surface as a source for
903 tropospheric nitrous acid, *Nature Geoscience*, 4, 440-443, 10.1038/ngeo1164, 2011.

904